



Review

# Hydrogel-Based Energy Harvesters and Self-Powered Sensors for Wearable Applications

Zhaosu Wang<sup>1</sup>, Ning Li<sup>1</sup>, Zhiyi Zhang<sup>2</sup>, Xiaojing Cui<sup>3,\*</sup> and Hulin Zhang<sup>1,\*</sup>

<sup>1</sup> College of Electronic Information and Optical Engineering, Taiyuan University of Technology, Taiyuan 030024, China

<sup>2</sup> College of Materials Science and Engineering, Taiyuan University of Technology, Taiyuan 030024, China

<sup>3</sup> School of Physics and Information Engineering, Shanxi Normal University, Taiyuan 030031, China

\* Correspondence: 20210084@sxnu.edu.cn (X.C.); zhanghulin@tyut.edu.cn (H.Z.)

**Abstract:** Collecting ambient energy to power various wearable electronics is considered a prospective approach to addressing their energy consumption. Mechanical and thermal energies are abundantly available in the environment and can be efficiently converted into electricity based on different physical effects. Hydrogel-based energy harvesters have turned out to be a promising solution, owing to their unique properties including flexibility and biocompatibility. In this review, we provide a concise overview of the methods and achievements in hydrogel-based energy harvesters, including triboelectric nanogenerators, piezoelectric nanogenerators, and thermoelectric generators, demonstrating their applications in power generation, such as LED lighting and capacitor charging. Furthermore, we specifically focus on their applications in self-powered wearables, such as detecting human motion/respiration states, monitoring joint flexion, promoting wound healing, and recording temperature. In addition, we discuss the progress in the sensing applications of hydrogel-based self-powered electronics by hybridizing multiple energy conversion in the field of wearables. This review analyzes hydrogel-based energy harvesters and their applications in self-powered sensing for wearable devices, with the aim of stimulating ongoing advancements in the field of smart sensors and intelligent electronics.



**Citation:** Wang, Z.; Li, N.; Zhang, Z.; Cui, X.; Zhang, H. Hydrogel-Based Energy Harvesters and Self-Powered Sensors for Wearable Applications. *Nanoenergy Adv.* **2023**, *3*, 315–342. <https://doi.org/10.3390/nanoenergyadv3040017>

Academic Editors: Ya Yang, Dukhyun Choi and Zhong Lin Wang

Received: 28 August 2023  
Revised: 9 October 2023  
Accepted: 10 October 2023  
Published: 16 October 2023



**Copyright:** © 2023 by the authors. Licensee MDPI, Basel, Switzerland. This article is an open access article distributed under the terms and conditions of the Creative Commons Attribution (CC BY) license (<https://creativecommons.org/licenses/by/4.0/>).

**Keywords:** hydrogel; triboelectric; piezoelectric; thermoelectric; wearable; energy harvester; self-powered; sensor

## 1. Introduction

Wearable electronics have stood out as a prominent field of research and development over the past few years, driven by the growing demand for portable and interactive devices [1–4]. However, the limited lifespan of batteries and the inconvenience of frequent charging have posed significant challenges to the widespread adoption of wearable technology [5–8]. To address these challenges, researchers have turned their attention toward self-powered energy harvesting technologies, aiming to utilize ambient energy sources for sustainable power generation [9–12]. Among various energy harvesting approaches, hydrogel-based energy harvesters have emerged as a promising solution due to their unique properties, such as excellent flexibility, conformance to irregular surfaces, and biocompatibility [13,14]. Hydrogels, which are crosslinked networks of hydrophilic polymers, have been widely explored to achieve energy conversion through various mechanisms, including triboelectric nanogenerators (TEGs) [15,16], piezoelectric nanogenerators (PENGs) [17], and thermoelectric generators (TEGs) [18,19].

TEGs are based on the triboelectric effect, which involves the generation of electrical charges through the contact and separation of different materials [20]. These devices utilize friction-induced charge transfer to harvest energy from human motion, mechanical vibrations, or other ambient movements. The development of wearable TEGs has

revolutionized the concept of energy harvesting by enabling continuous power supply from everyday activities, such as walking [21], running [22], or even typing on a keyboard [23]. Similarly, PENGs utilize the piezoelectric effect, which converts mechanical strain or pressure into electrical energy [24]. These nanogenerators can be integrated into wearable sensors or garments to generate power from body movements, such as bending, stretching, or applying external forces. The versatility of PENGs allows for their integration into various wearable applications, including health monitoring [25], motion tracking [26], and human–machine interfaces [27]. Another promising energy harvesting technology refers to thermoelectric generators, which can convert temperature gradients into electrical energy [28]. By utilizing temperature differences between the human body and the surrounding environment, thermoelectric cells can harvest energy from the heat dissipated by the body [29]. This sustainable approach provides a constant power source for wearable devices, eliminating the need for external power supplies or battery replacements. Further, the intrinsic temperature-sensitive characteristics of thermoelectric devices have led to a plethora of temperature sensors based on the thermoelectric effect [30,31]. The self-powered nature of these energy-harvesting technologies not only enhances the usability and convenience of wearable electronics but also opens up new opportunities for diverse applications. For instance, self-powered wearable sensors and health-monitoring devices can autonomously track vital signs, such as heart rate [32] or respiratory rate [33], without the need for frequent battery charging. Additionally, self-powered wearable technology enables the development of innovative applications in augmented reality, virtual reality, and smart robots [34–36].

So far, various energy-harvesting strategies have been generally discussed, including mechanical and thermal energy harvesting, and there is no lack of energy storage methods, such as self-charging supercapacitor power cells [37,38]. For sensing functions, there have been reviews on self-powered sensors based on TENGs and PENGs [39], or nanogenerators for sensing applications in limited application scenarios [40], as well as chemical sensing applications regarding, for example, gas sensors [41]. Hydrogel, as a research hotspot in recent years, is flexible and stretchable, and can also have multiple properties such as biocompatibility, degradability, and self-healing. Hydrogel can be combined with a variety of energy-harvesting methods to form many hydrogel devices. Due to their inherent excellent properties, compared with traditional rigid materials, hydrogels with good electrical conductivity and mechanical properties can be well-adapted to wearable applications to detect human body temperature, pulse, respiration, and movement status. Hydrogel devices are showing more and more advantages in the field of wearable electronics. Hence, here, hydrogel devices are introduced as an entry point for studies in energy harvesting and self-powered sensing applications in wearable scenarios.

In this mini-review, we aim to explore the design principles, performance characteristics, and self-powered applications of hydrogel-based energy harvesters that utilize key technologies of TENGs, PENGs, and TEGs. Additionally, we will present the latest research outcomes in the field of self-powered wearable sensors that combine multiple energy-harvesting effects. Furthermore, we will delve into the challenges and future prospects of these energy-harvesting systems, aiming to inspire further research and development in the field of self-powered wearable electronics.

## 2. Hydrogel-Based TENGs

### 2.1. Hydrogel-Based TENGs for Energy Harvesting

TENGs have shown great potential in the fields of ambient energy harvesting and multi-function sensing [42–46]. However, research on TENGs that are completely flexible and environmentally friendly is still limited. Hydrogels can be prepared from natural or synthetic polymers and can form various components of stretchable devices [47]. In the following sections, several studies will be presented to showcase hydrogel-based TENGs as energy harvesters.

When using hydrogels as electrodes in TENGs, the most commonly used configuration is the single-electrode mode due to its fabrication simplicity. For example, Figure 1a presents the design of a single-electrode mode TENG, named MH-TENG, which incorporates mixed MXene nanosheets and polyvinyl alcohol (PVA) hydrogel as flexible and stretchable electrodes [48]. In order to protect the composite hydrogel from moisture loss, a silicon rubber Ecoflex layer was utilized as a triboelectric component (Figure 1a(i)). The MXene/PVA hydrogel in the MH-TENG serves as both an electrode and a provider of ion transport, enabling electrostatic screening of triboelectric charges in the Ecoflex. It is worth noting that the incorporation of MXene nanosheets serves two purposes: improving the stretchability of the PVA hydrogel by acting as a crosslinker and facilitating the formation of microchannels that enhance the transport of positive ions within the complex hydrogel after triboelectrification. This synergistic effect significantly enhances the overall output of the MH-TENG (Figure 1a(ii)). The optimum output power density of the MH-TENG is  $0.33 \text{ W m}^{-2}$  for a load resistance of  $109 \Omega$ . Subsequently, the performance of the MH-TENG was evaluated by attempting to illuminate multiple light-emitting diodes (LEDs). Remarkably, a total of 40 LEDs were effortlessly illuminated by simply tapping the MH-TENG with bare hands (Figure 1a(iii,iv)). This successful demonstration highlights the significant potential of the design for harvesting low-frequency mechanical energy. This work demonstrates the advantages of MXene for improving the mechanical and electrical properties of PVA hydrogels and generating additional triboelectric output.

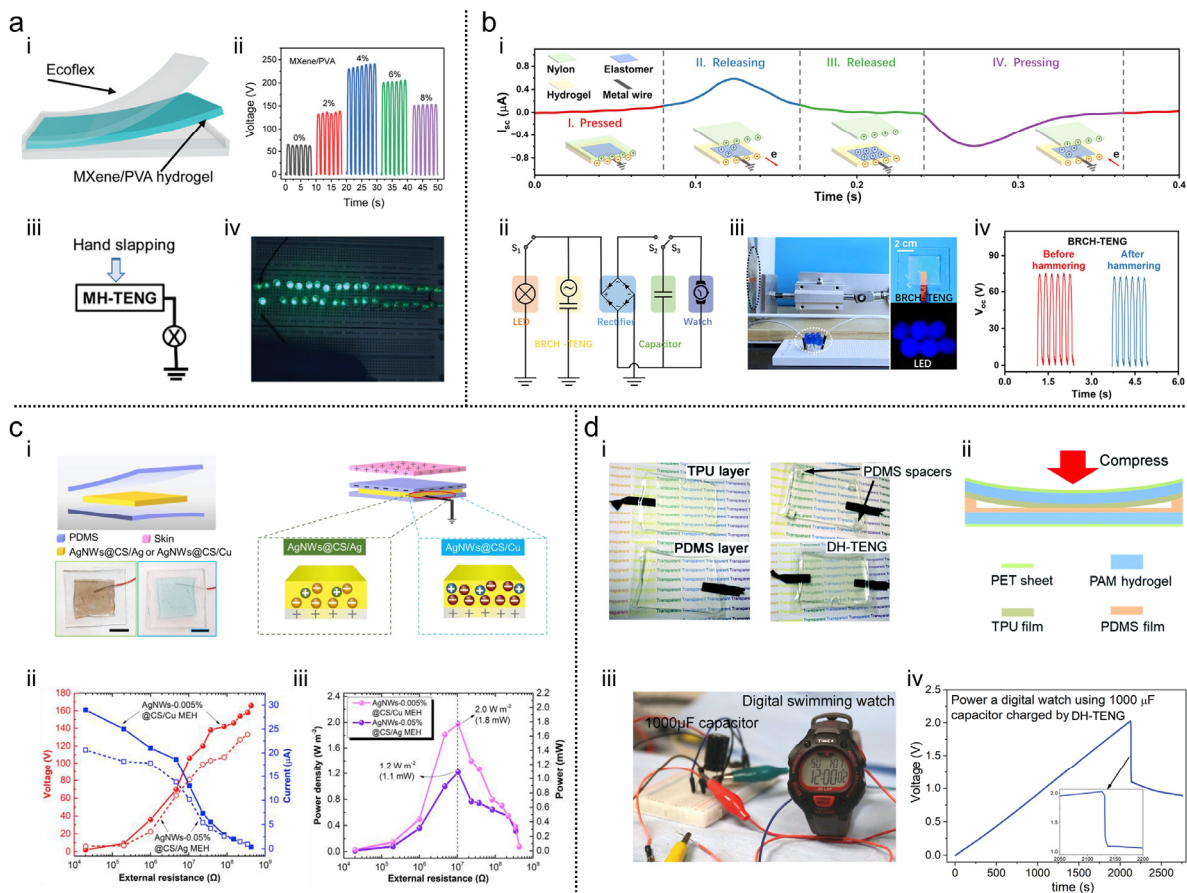


**Figure 1.** (a) Construction (i) and output performance for different concentrations of MXene (ii). Schematic and presentation of MH-TENG lighting LEDs (iii,iv). Reproduced with permission [48]. Copyright 2021, Wiley. (b) Working mechanism (i) and applications (ii–iv) of BRCH-TENG. (ii) Circuit of a self-charging system utilizing energy obtained from the TENG to charge electronics. (iii) Photos

demonstrating LED illumination by tapping TENG. (iv) Open-circuit voltage ( $V_{oc}$ ) measurement of the BRCH-TENG before and after hammering. Reproduced with permission [49]. Copyright 2023, Elsevier. (c) Schematic representation (i) and output (ii,iii) of AgNWs@CS/Ag and AgNWs@CS/Cu hydrogel motion energy harvesters. Reproduced with permission [50]. Copyright 2019, Elsevier. (d) Construction and energy harvesting of DH-TENG. Digital photo (i) of the DH-TENG and schematic of the contact–separation operating mode (ii). Photo (iii) and voltage signal (iv) of a watch powered using a capacitor charged with the TENG. Reproduced with permission [51]. Copyright 2020, Royal Society of Chemistry.

Li et al. successfully prepared a breakage-resistant conductive hydrogel (BRC hydrogel) with remarkable mechanical reliability using a solvent exchange strategy. Then, they fabricated a BRC hydrogel-based TENG (BRCH-TENG) similarly in the single-electrode mode [49], as depicted in Figure 1b. For this configuration, a VHB<sup>TM</sup> elastomer served as the negative tribo-material, while a nylon film was used as the positive tribo-material (Figure 1b(i)). When they constructed a BRCH-TENG with a  $40 \times 40 \text{ mm}^2$  electrode area using the elastomer and hydrogel electrodes, it yielded a maximal short-circuit current ( $I_{sc}$ ) of  $0.59 \mu\text{A}$ . The power density can reach  $57.5 \text{ mW/m}^2$  with a matching resistance of  $100 \text{ M}\Omega$ . Furthermore, a self-charging system consisting of the BRCH-TENG, capacitors, and electronics was established (Figure 1b(ii)). By closing switch  $S_1$ , the BRCH-TENG could power serially connected LEDs through continuous tapping (Figure 1b(iii)). When closing switch  $S_2$ , the BRCH-TENG could charge capacitors, while switch  $S_3$  allowed the collected energy to be utilized for driving electronics. Moreover, even after undergoing over 5000 cycles of beatings and enduring significant external forces, the BRCH-TENG exhibited no discernible damage and maintained its initial electrical output performance (Figure 1b(iv)). This enhanced mechanical resilience can be attributed to the breakage resistance of the hydrogel electrode in the BRC hydrogel-based TENG, ensuring improved safety and durability. Although the output power density of this work is not as high as that of the prior one, it demonstrates the durability of conductive hydrogel electrodes prepared with a solvent exchange strategy exploiting the Hoffmeister effect.

Ion-conducting hydrogels tend to be biocompatible, light transmissive, and elastic. To strengthen the conductivity of hydrogels, composite hydrogel networks with mixed ionic/electronic conduction, derived from chitosan (CS) crosslinked by  $\text{Ag}^+/\text{Cu}^{2+}$ , and embedded with Ag nanowires (AgNWs), were developed for efficient mechanical energy collecting, as shown in Figure 1c [50]. These composites are specifically referred to as AgNWs@CS/Ag and AgNWs@CS/Cu. A sandwich-structured device was fabricated, comprising a polydimethylsiloxane (PDMS) layer as the contact electrification layer and hydrogels as the current collectors (Figure 1c(i)). The concentration of AgNWs in the hydrogels was found to have a significant influence on the device's output. Higher conductivity in both sets of hydrogel networks led to increased output. Notably, due to the higher concentration of  $\text{Ag}^+$  ions compared with  $\text{Cu}^{2+}$  ions, the electric double layer (EDL) in AgNWs@CS/Ag exhibited a thinner thickness compared with AgNWs@CS/Cu. Consequently, the capacitance ( $C$ ) of the EDL in AgNWs@CS/Ag was greater. Using the equation  $C = Q/V$ , where  $Q$  represents the quantity of induced charges in the EDL resulting from contact-separation between PDMS and the skin, which remains constant, resulted in a higher output level of AgNWs@CS/Cu (Figure 1c(ii,iii)). The maximum power density of AgNWs@CS/Cu harvester was  $2 \text{ W m}^{-2}$  at an external resistance of  $10.5 \text{ M}\Omega$ . This study demonstrates the introduction of metal ions and AgNWs to synergistically increase the conductivity of hydrogels.

In the majority of cases, TENGs are typically fabricated in single-electrode mode with the external circuit grounded. In theory, a single-electrode TENG can only achieve one-half the output compared with a dual-electrode TENG of the same materials. Furthermore, the output performance of single-electrode TENGs relies on the triboelectric properties of materials with which they are in contact, severely limiting the applicability. To address these limitations, Jing et al. developed a dual-electrode hydrogel-based TENG (DH-TENG) utilizing polyacrylamide (PAM) hydrogels with embedded NaCl as electrodes, as shown in

Figure 1d [51]. The DH-TENG consists of a thermoplastic polyurethane (TPU) layer and a polydimethylsiloxane (PDMS) layer, both of which exhibit high transparency (Figure 1d(i)). PET sheets are used to provide sufficient force for the DH-TENG to swiftly recover once the compression force is removed (Figure 1d(ii)). Under compression with a periodic force of 6 N, the TENG can achieve a maximum instantaneous voltage of 311.5 V. A peak power density of  $2.7 \text{ W m}^{-2}$  can be realized with a  $4.7 \text{ M}\Omega$  resistor. To harness the generated energy, the DH-TENG was used to charge various capacitors with a bridge rectifier. Afterward, the stored energy was used to power small electronics. For instance, a  $1000 \mu\text{F}$  capacitor charged with the DH-TENG successfully powered a digital watch (Figure 1d(iii)). Analysis of the corresponding voltage data revealed an initial sharp voltage drop of approximately 1 V upon activating the digital watch. Following this initial drop, the watch was continuously powered, with energy consumption slightly exceeding the charging rate of the DH-TENG (Figure 1d(iv)). This demonstration clearly indicates that the DH-TENG is highly efficient in converting mechanical motion into electrical energy, enabling it to effectively power small devices. At the same time, this particular highly transparent design has the potential to be effective in application scenarios with special needs.

In conclusion, hydrogel-based TENGs have emerged as a promising direction for achieving ultra-flexible devices and have proven to be capable of efficiently capturing mechanical energy and converting it into electrical energy, highlighting their tremendous potential as viable power sources. Furthermore, TENGs are characterized by high voltage and small current, which means that their output energy and energy utilization efficiency are not high. Therefore, an efficient energy management scheme plays an important role in further exploiting the practical applications of TENGs. There have been approaches utilizing transformers, mechanical/electronic switches, and more recently, strategies for coupling charge pump circuits to BUCK circuits [52]. It is also possible to combine supercapacitors to store the energy collected by TENGs [53]. The utilization of energy management strategies for hydrogel-based TENGs is a perspective to drive their improvement.

## 2.2. Self-Powered Applications of Hydrogel-Based TENG Devices

Flexible TENGs have emerged as a promising approach to solving the challenges of energy supply for intelligent electronics while offering multifunctional sensing capabilities [54–58]. These self-powered sensors have garnered significant interest in flexible wearable electronics. The rapid advancement of virtual reality technologies has propelled the exploration and development of flexible TENGs for diverse applications in the realm of wearable smart electronics and human–machine interfaces.

Implantable and wearable transient electronics based on TENGs have found applications in various fields such as self-powered sensing and electrical-stimulation therapy. However, the current devices have limited adaptation to human tissue shapes, and their degradation rate is generally unsatisfactory. To improve this situation, Li et al. utilized PEGDA and Laponite nanocomposites (Lap) to fabricate hydrogels. Additionally, they developed a flexible biodegradable single-electrode TENG (BS-TENG) by assembling the components [59]. The BS-TENG exhibited excellent skin-fit properties, allowing it to generate varying electrical signals when subjected to mechanical deformation. As shown in Figure 2a, this enabled accurate attachment of the device to the neck, wrist, and fingers, thereby serving as a self-powered sensor for real-time detection of respiration, joint movement, and other physiological parameters of the body. Significantly, the device can be downgraded in a controlled manner. Thus, the design is poised to become the mainstay in diagnostic and therapeutic applications, playing a vital role in the field of biomedical science.

In addition to monitoring physiological indicators, studies have also implemented monitoring exercise status and displaying the results on commonly used cell phones. Zhang et al. presented a hydrogel named PTSM, composed of PAM, tannic acid (TA), sodium alginate (SA), and MXene [60]. Specifically, PAM/SA was used as a framework for the dynamic network hydrogel, while the addition of TA significantly enhanced its mechanical

properties through the formation of a robust hydrogen bond with PAM/SA. MXene, with its high density of hydrophilic functional groups, facilitated uniform distribution within the hydrogel and the establishment of conductive pathways. The resulting hydrogel exhibited exceptional self-healing capabilities, rendering it highly suitable for utilization as an electrode in PTSM-TENGs. The construction of the PTSM-TENG is illustrated in Figure 2b(i), where the PTSM hydrogel is encapsulated with Ecoflex silicone rubber. The PTSM-TENGs exhibited remarkable long-term durability, efficient energy collection, and outstanding tactile sensing performance. A wireless motion monitoring system was developed to expand the functionality of motion sensing, integrating a wireless transmission circuit and a cell phone application. Upon affixing TENGs to clothing, the generated electrical signals during movement were wirelessly transmitted to the application software for display using Bluetooth (Figure 2b(ii,iii)). This successful demonstration highlights the enormous potential of designed TENGs as wearable devices. The application software development in this study is also very much in line with the current trend in wearable devices.

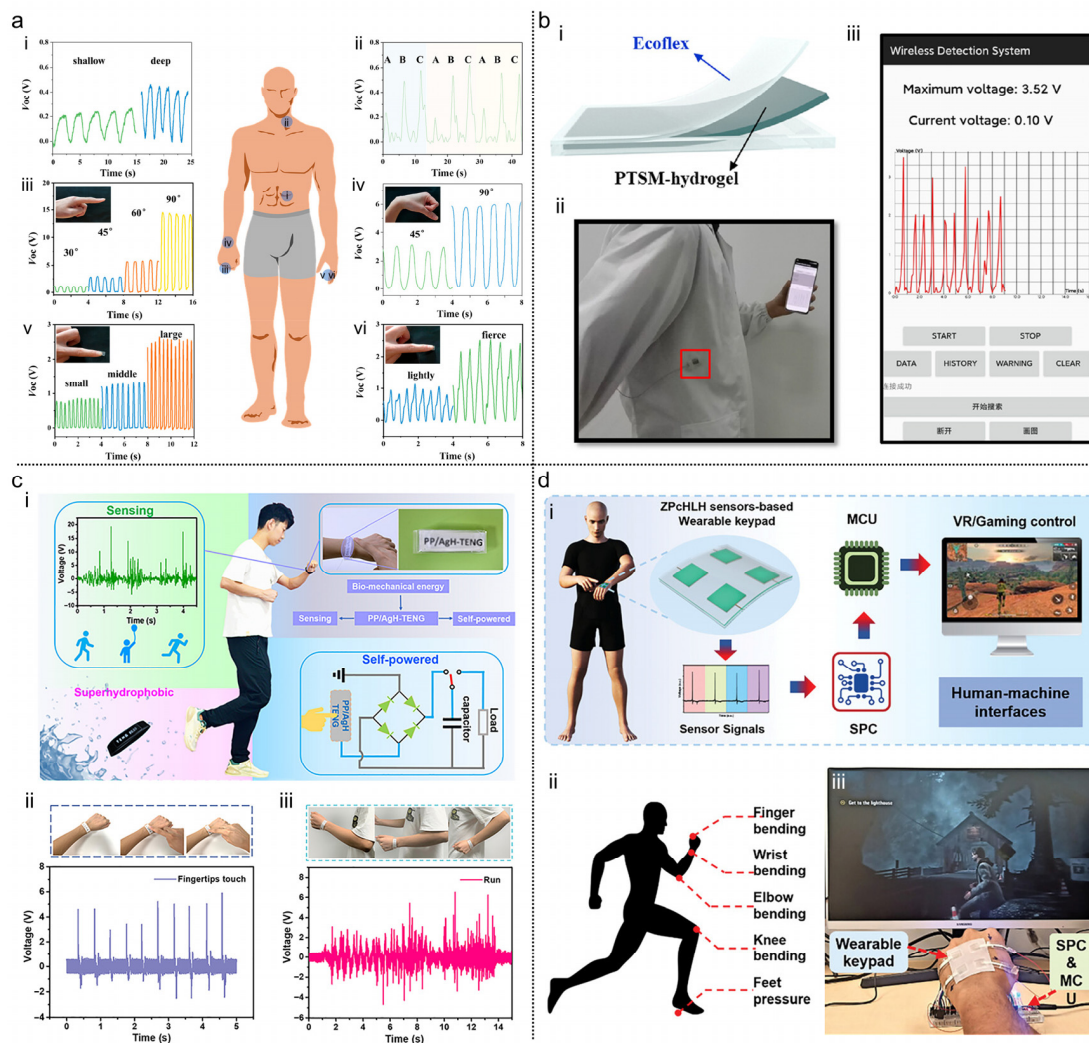


**Figure 2.** (a) Physiological signals and joint motion sensing of TENGs. (i) Respiratory detection by mounting the TENG on the belly. (ii)  $V_{oc}$  of pronunciation of “A”, “B”, and “C”.  $V_{oc}$  of the TENG attached to the finger (iii) and the wrist (iv).  $V_{oc}$  of the TENG with (v) finger swiping and (vi) tapping. Reproduced with permission [59]. Copyright 2023, American Chemical Society. (b) Application of PTSM-TENG as a wireless motion monitoring device. (i) Schematic structure. (ii) Photograph of PTSM-TENG (location marked by the red box) attaching to the body for wireless motion sensing. (iii) Real-time display interface for the mobile terminal. Reproduced with permission [60]. Copyright 2023,

American Chemical Society. (c) Application of PP/AgH-TENGs. (i) Schematic representation of the PP/AgH-TENG-designed wristband. When wearing the self-powered sensing wristband, fingertip touch (ii) and running (iii) drive the generation of output voltage. Reproduced with permission [61]. Copyright 2022, American Chemical Society. (d) Self-powered wearable applications of ZPcHLH-TENGs. (i) System architecture schematic of the wearable keypad for real-time control of games. (ii) Demonstration of the keypad as an HMI for gaming control. (iii) Illustration of biomotion sensing points. Reproduced with permission [62]. Copyright 2023, Wiley.

Similarly, for sports monitoring, the following study designed devices closer to the sports bracelet for daily use. Qu et al. developed a superhydrophobic TENG, referred to as PP/AgH-TENG, by integrating the PDMS film surface modified with polytetrafluoroethylene (PTFE) particles as the triboelectric layer. The AgNWs/PVA hydrogel served as the electrode [61]. The resulting TENG exhibited remarkable transparency and superhydrophobicity. To harness these attributes, a self-powered bracelet was designed using 3D printing (Figure 2c(i)). This innovative bracelet serves the dual purpose of collecting energy from human movement and detecting activities. When the dial is touched with the fingertips, a corresponding output voltage is generated (Figure 2c(ii)). This electrical signal not only activates the dial but also stores the electricity produced by each touch, subsequently powering the bracelet itself. Similarly, during regular bodily movement, relative motions between the bracelet and the body induce inductive charging. Analysis of the output voltage generated during running reveals that the electrical signal displays considerable variability and frequency fluctuations, primarily attributable to the irregular changes in wrist rhythm and strength while running (Figure 2c(iii)). The specially designed bracelet seamlessly captures and converts energy from bodily movement in real time. The converted energy can be stored within the bracelet to serve as a power source. Additionally, the size and frequency of the generated signals during the energy harvesting process provide valuable insights into monitoring human movement. Hence, the TENG used in their study exhibits exceptional self-powered sensing performance. Meanwhile, one of the features of the TENG in their study is that it adopts the design of a sports bracelet. The device form factor is also significant in the wearable domain.

Despite monitoring physiological information and movement, hydrogel-based TENGs can also be used for human-computer interaction. Zeolitic imidazolate framework-8 (ZIF-8), a metal-organic framework (MOF), can be incorporated into hydrogels as an enhanced nanofiller, creating a strongly stretchable, flexible, and durable electrode. A ZIF-8-enhanced LiCl-containing polyacrylamide-co-hydroxyethyl acrylate (PAAm-co-HEA) hydrogel, has been successfully fabricated [62]. The hydrogel-based TENG device is called ZPcHLH-TENG. A wearable keypad system was created using an array of ZPcHLH-TENGs (Figure 2d(i)). The signals produced by the keypad underwent initial filtration through low-pass RC filters to remove noise. The amplified signals were then passed through an amplifier circuit to increase their amplitude. Subsequently, these amplified signals were received by a microcontroller (ESP32). To enable real-time interaction with a computer game, a custom Python script was implemented on a desktop computer to read the inputs and establish communication with the desktop. This allowed for the real-time transmission of commands to control the game "Alan Wake" (Figure 2d(ii)). The successful utilization of this wearable interfacing system demonstrates the potential application of ZPcHLH-TENG sensors in human-machine interfaces (HMIs) for virtual reality (VR) games and electronic skin (e-skin). Furthermore, ZPcHLH-TENG devices exhibited excellent sensitivity when testing bending movements across different body regions, effectively serving as biometric motion sensors (Figure 2d(iii)). Currently, many hydrogel TENGs realize motion sensing, while this example work brings refreshing game control applications that have great significance in human-computer interaction.

Hydrogel-based TENGs have been utilized in wearables for monitoring various physiological parameters such as respiration, different body part bending motions, and movement states. They also serve as self-powered wearable human-machine interfaces (HMIs). The incorporation of flexible hydrogels allows traditional rigid TENGs to be more effec-

tively applied to the human body, enabling seamless integration between the device and the wearer.

### 3. Hydrogel-Based PENGs

#### 3.1. Hydrogel-Based PENGs for Energy Harvesting

The rapid advancement of wearable electronic systems necessitates a sustainable energy source capable of extracting energy from the surrounding environment without frequent recharging. Piezoelectric nanogenerators (PENGs) offer a potential solution by converting irregular and scattered mechanical energy from the environment into electrical energy, providing a long-term and continuous power supply for mobile distributed electronic devices [63–65]. In the realm of piezoelectric materials, polyvinylidene fluoride (PVDF) and its copolymers have garnered attention for their unique electrical properties, high flexibility, excellent mechanical processability, and long-term stability, making them promising materials for PENGs [66–69]. In the subsequent discussion, we will present two hydrogel-based PENG devices that utilize PVDF.

Polyvinylidene fluoride (PVDF) is widely recognized for its outstanding mechanical properties, piezoelectric behavior, and biocompatibility. Among its various phases, the  $\beta$ -phase, characterized by a noncentrosymmetric polar structure, exhibits specific piezoelectric properties. Figure 3a(i) depicts the construction of a piezoelectric PVA/PVDF hydrogel using a four-stage process involving freezing/thawing, solvent replacement, annealing, and swelling [70]. In the first stage, the gel was formed after two freeze/thaw cycles in dimethyl sulfoxide (DMSO). Following this, the gel was soaked in distilled water to replace DMSO. In the subsequent stage, the obtained hydrogel was annealed and swelled in distilled water. This elaborate process enhanced the intermolecular interaction within the PVA/PVDF gel, thereby facilitating the formation of the electroactive  $\beta$ -phase of PVDF. To evaluate the piezoelectric response, the sensitivity of the PVA sample to acceleration was measured, resulting in a  $V_{pp}$  sensitivity of 0.086 and a fitting correlation coefficient ( $R^2$ ) of 0.972. Conversely, the PVA/PVDF composite hydrogel exhibited increased sensitivity to acceleration, with a sensitivity of  $V_{pp}$  at 0.432 and an  $R^2$  value of 0.965 (Figure 3a(ii)). This comparison suggests that the hydrogel displayed greater sensitivity to forces. Furthermore, the effectiveness of piezoelectric signal generation was illustrated by the fact that  $V_{pp}$  is equal when the leads are connected positively or negatively (Figure 3a(iii)). Further investigation of the piezoelectric characteristics of the hydrogel used piezo-response force microscopy (PFM). The PFM analysis revealed a substantial piezoelectric response across a significant area, surpassing even the response observed in the PVDF phase during phase mapping. This finding serves to reinforce the robust hydrogen bonding interaction between PVA and PVDF, thus promoting the forming of the  $\beta$ -phase PVDF. Additionally, the alternating voltage signal generated by the hydrogel was rectified using a rectifier (Figure 3a(iv)). The rectified signal was used to charge a capacitor. After a charging duration of approximately 5 min, the capacitor had stored enough power to supply the LED. This work demonstrates collecting mechanical energy by integrating a classical piezoelectric material, PVDF, into a hydrogel, thus obtaining a piezoelectric hydrogel. It also provides an idea for preparing a piezoelectric hydrogel, that is, doping piezoelectric materials into the hydrogel carrier.

The mechanical properties and piezoelectric sensitivity of piezoelectric devices can be enhanced with morphology tuning of nanofibers. Chen et al. developed a self-powered electrical-stimulator-based wound dressing (SEWD) consisting of two layers: a top piezoelectric layer composed of tree-like P(VDF-TrFE) nanofibers, prepared with electrospinning, and a lower layer made of Fe ions and catechol group-based adhesive PAM-gelatin hydrogel (Figure 3b(i)) [71]. The electrospinning process was used to control the microstructure of P(VDF-TrFE) nanofiber, inspired by the large motion amplitude observed in nature when trees sway in the wind. By adjusting the electrical conductivity of the electrospinning solution, a tree-like bionic structure was achieved, exhibiting enhanced mechanical and piezoelectric properties compared with traditional P(VDF-TrFE) films. The tree-like

nanofibers sensitized mechanical stimulation from small activities, converting them into electrical signals that were transmitted to the wound, enabling electrical stimulation (ES) therapy. Inspired by marine mussels, the hydrogel utilized the redox electron pairs formed by catechol and metal ions. This bionic material demonstrated electrical activity compatible with tissues, allowing for the conduction of electrical signals generated by the piezoelectric effect to the wound site for effective ES treatment during tissue repair. A schematic diagram of the piezoelectric effect is shown in Figure 3b(ii). The open-circuit voltage (OCV) of the P(VDF-TrFE) nanofibers was measured under different pressures, revealing a stable response with a voltage of about 0.3 V observed at a force of 0.1 N, indicating sensitivity to small external forces (Figure 3b(iii)). The output voltage increased gradually with increasing force. Dendritic fibers exhibited higher crystallinity due to the increased mechanical stretching during the electrospinning process, favoring the crystallization of P(VDF-TrFE) and resulting in improved piezoelectric properties. These findings highlight the favorable application potential of the prepared tree-like nanofibers.

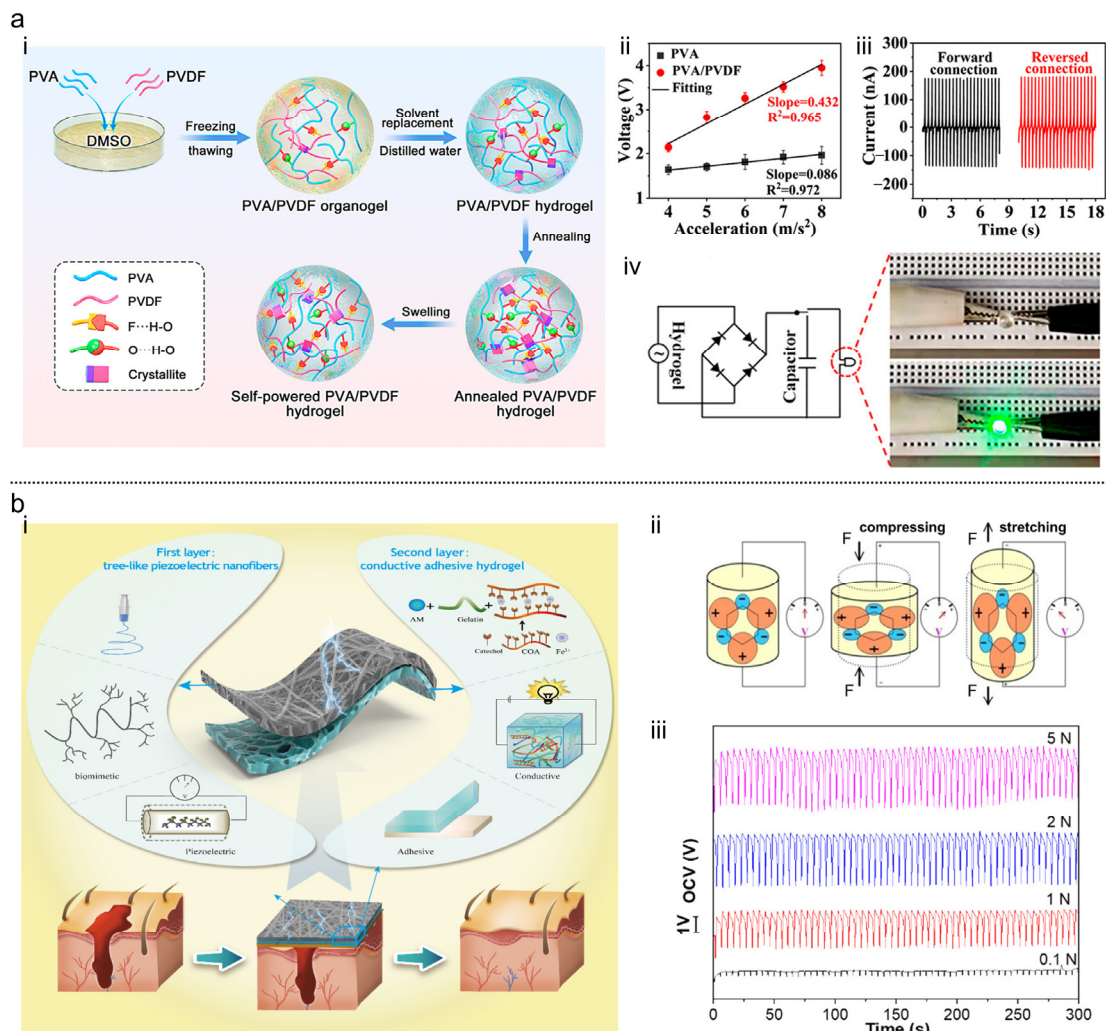


**Figure 3.** (a) Preparation and piezoelectric properties of PVA/PVDF hydrogel. (i) Scheme of the preparation process. (ii) Dependence of  $V_{pp}$  on acceleration. (iii)  $V_{pp}$  of positive and negative connections. (iv) Bridge rectifier circuit diagram and lighting LED with PVA/PVDF hydrogel. Reproduced with permission [70]. Copyright 2022, American Chemical Society. (b) Preparation and piezoelectric response of a two-layered SEWD. Schematic diagram of a SEWD (i) and the piezoelectric effect (ii). The arrows indicate the direction of the forces. (iii) OCV curves at different pressures. Reproduced with permission [71]. Copyright 2023, American Chemical Society.

The above two energy harvesting devices, based on the piezoelectric effect, exhibit good piezoelectric performance. The first device involves a piezoelectric hydrogel, while the second design utilizes hydrogels as electrodes. Both designs demonstrate promising piezoelectric capabilities. The following section discusses the self-powered wearable applications of these two piezoelectric devices.

### 3.2. Self-Powered Applications of Hydrogel-Based PENG Devices

Electrical stimulation has been used to modulate the morphology, state, membrane permeability, and life cycle of cells for therapeutic purposes in various diseases, including trauma, degenerative disorders, tumors, and infections. Materials with piezoelectric properties can provide non-invasive electrical stimulation to cells, aiding in tissue regeneration [72–76]. Hence, these piezoelectric materials offer the potential to advance cell-based therapies and tissue engineering by delivering electrical stimulation in a minimally invasive manner. Both of the aforementioned piezoelectric devices have demonstrated self-powered applications that facilitate wound healing. In the following section, we will further elaborate on these applications.

The impact of the previously mentioned PVA/PVDF hydrogel (Figure 3a) on wound healing was investigated utilizing a diabetic Sprague Dawley (SD) rat full-thickness skin defect model [70]. The localized piezoelectric stimulation generated by piezoelectric hydrogels during bending was administered in real time to the wound bed through the physical activities of the rats. Figure 4a(i) illustrates the gradual changes in the wound area at various time points. Notably, no trace of overstimulation or infection was observed in any of the rats. As anticipated, the untreated wounds in the control group exhibited dryness and crust formation, while wounds treated with either PVA or PVA/PVDF hydrogel stayed relatively moist. From day 2 onwards, it became evident that wound closure occurred quicker in the composite hydrogel group. On day 8, the remaining wound in the composite hydrogel group was only 13.5% of the initial wound area, which was smaller in comparison with the PVA hydrogel group (41.4%) and the control group (58.6%). Complete closure of the skin wounds was achieved by day 10 in the composite hydrogel group, while wounds in the other groups remained non-healing. On day 14, unclosed wounds were still observed in the control group and the PVA hydrogel group, with the percentage of residual wound area being 19.0% and 11.0%, respectively. Furthermore, wound tracking analysis verified that the PVA/PVDF hydrogel group exhibited a substantially higher wound closure rate (Figure 4a(ii,iii)). These findings demonstrate that the PVA/PVDF piezoelectric hydrogel can promote wound closure significantly in diabetic rats. This may be due to its advantages of absorbing wound exudates and promoting cell proliferation.

The previously mentioned adaptive SEWD, as illustrated in Figure 3b, is designed for easy and painless application and removal on human skin. This feature makes it well-suited for addressing irregular wound surfaces and edges. Significantly, the SEWD proves to be highly effective in promoting wound healing, as evidenced by the findings presented in Figure 4b [71]. To evaluate the healing-promoting effect of the SEWD, full-thickness skin defects in SD rats were studied. In this experiment, the hydrogel component of the SEWD was chosen as the control group. Comparative examination of wound images and wound contours plotted at identical scales revealed significantly enhanced wound healing in the SEWD group (Figure 4b(i,ii)). The closure rate of the wounds in the SEWD group reached almost 80% within the first week, compared to 53% in the hydrogel control group and 36% in the gauze control group. By the second week, the wounds treated with SEWD had completely healed, while the control groups exhibited incomplete healing, with closure rates of only 60% and 81% for the control and hydrogel groups, respectively. The remarkable healing-promoting ability of the SEWD can be attributed to two factors. Firstly, the SEWD dressing, which primarily consists of biomass and possesses a bionic structure, creates an optimal environment for wound healing. Secondly, the SEWD's healing-promoting effect is augmented by the electric stimulation (ES) generated by the piezoelectric layer. Through postoperative activities, the rats effectively stimulated the piezoelectric layer, triggering the

generation of electrical signals that were then transmitted to the surrounding skin tissue through the conductive hydrogel. This electrical stimulation promoted cell proliferation and accelerated wound healing.

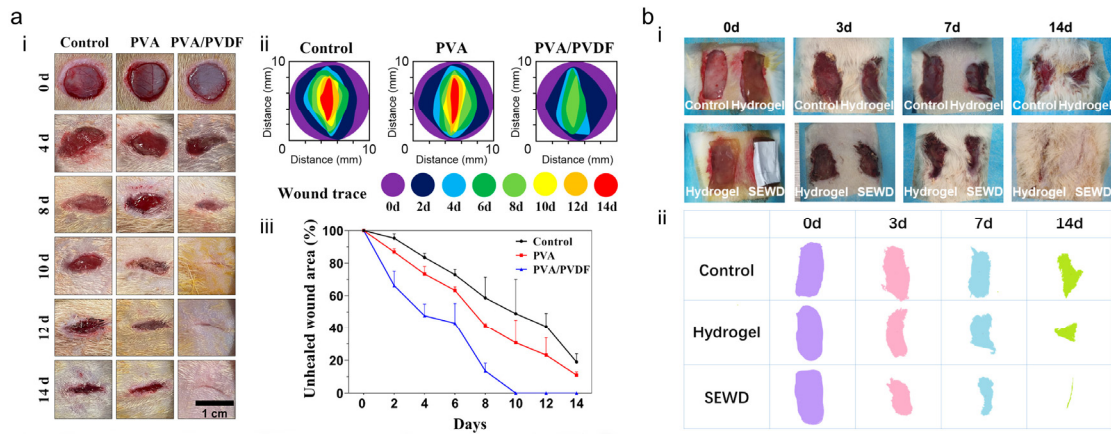


**Figure 4.** (a) Promotion of wound healing in diabetic rats using PVA/PVDF hydrogel. (i) Photos of wounds in diabetic SD rats at different time points. (ii) Wound tracking analysis after surgery. (iii) Curves of the percentage of remaining wound area to initial wound area and treatment time. Reproduced with permission [70]. Copyright 2022, American Chemical Society. (b) Promotion of full-thickness wound healing using SEWD. (i) Photos of the healing process of the wounds. (ii) Images of wounds at different time points. Reproduced with permission [71]. Copyright 2023, American Chemical Society.

The above-mentioned works showcase the application of hydrogel-based piezoelectric devices in promoting wound healing. The fusion of piezoelectric materials with flexible and stretchable biocompatible hydrogels has led to the development of diverse wearable piezoelectric devices, which hold tremendous potential in the field of medicine. This integration offers a novel healing strategy for effectively treating skin injuries, holding significant importance in the rapid, safe, and efficient promotion of wound healing.

## 4. Hydrogel-Based TEGs

### 4.1. Hydrogel-Based TEGs for Energy Harvesting

When a thermal gradient is introduced, mobile charge carriers (electrons and holes) in the material diffuse to the colder side, causing the accumulation of charge and a potential difference. This phenomenon is known as the Seebeck effect, and the potential difference produced per unit temperature difference is referred to as the Seebeck coefficient [77,78]. Thermoelectric devices based on semiconductor materials typically exhibit Seebeck coefficients in the range of tens to hundreds of microvolts per Kelvin, limiting their efficiency at or near ambient temperature [79–83]. The following highlights the work on hydrogel-based thermoelectric devices in terms of thermal energy harvesting. These devices not only offer better thermoelectric conversion capabilities than traditional thermoelectric materials but also possess advantages such as flexibility, stretchability, self-healing, and environmental friendliness.

Previous experiments have demonstrated that doping Se into the traditional thermoelectric material  $\text{Bi}_2\text{Te}_3$  can significantly enhance its Seebeck coefficient [84,85]. As illustrated in Figure 5a, based on  $\text{Bi}_2\text{Se}_{0.3}\text{Te}_{2.7}$ , an inorganic thermoelectric material, Li et al. presented a self-healing thermoelectric hydrogel, referred to as PAAc/XG/ $\text{Bi}_2\text{Se}_{0.3}\text{Te}_{2.7}$ , for continuous electricity production [86]. The hydrogel matrix, polyacrylic acid (PAAc), serves as a superabsorbent and hydrophilic polymer commonly used for self-healing due to its carboxyl functionality facilitating hydrogen bonding for repairing broken hydrogels. Xanthan gum (XG), an edible natural biopolymer, significantly enhances the mechanical strength of the hydrogel through molecular chain entanglement and hydrogen bonding, thanks to its

elongated molecular chains and multiple side chains. The hydrogel is synthesized with in situ polymerization, resulting in an optimal combination of self-healing characteristics and mechanical strength. Upon rejoining the damaged hydrogel, rapid recovery of the electrical performance is achieved, exhibiting a fast self-healing capability that restores the initial electrical conductivity within 2 s with no external stimulus. The self-healed hydrogel demonstrates excellent mechanical strength and stretchability, with the ability to be extended up to two times its original length (Figure 5a(i)). Compared with the initial hydrogel with a maximal stress of 0.033 MPa and a maximal strain of 482%, the self-healed sample can achieve maximal stress and strain of 0.018 MPa and 256%, respectively, resulting in 53% recovery. The  $V_{oc}$  and output power of the self-healed hydrogel after 12 h of healing were measured at  $-17.2$  mV and 38.0 nW, respectively, with a 40 K temperature difference (Figure 5a(ii)). This represents a decrease of 3.9% and 0.3%, respectively, compared with the initial (before being cut) samples. To evaluate the power generation capability of the hydrogel for flexible thermoelectric devices, a single-leg device was fabricated by connecting copper electrodes to the hydrogel. One end of the hydrogel contacts the skin surface, while the other end is exposed to the air, resulting in a temperature difference of 9.7 K and a generated voltage of 4.4 mV (Figure 5a(iii)). This novel thermoelectric material efficiently converts low-grade waste heat into electricity, presenting promising prospects for advancements in thermoelectric materials research. The designed thermoelectric hydrogel has good self-healing properties and has the potential to recover even after breakage. This advantage is to be further verified when wearing the hydrogel devices on the human body.

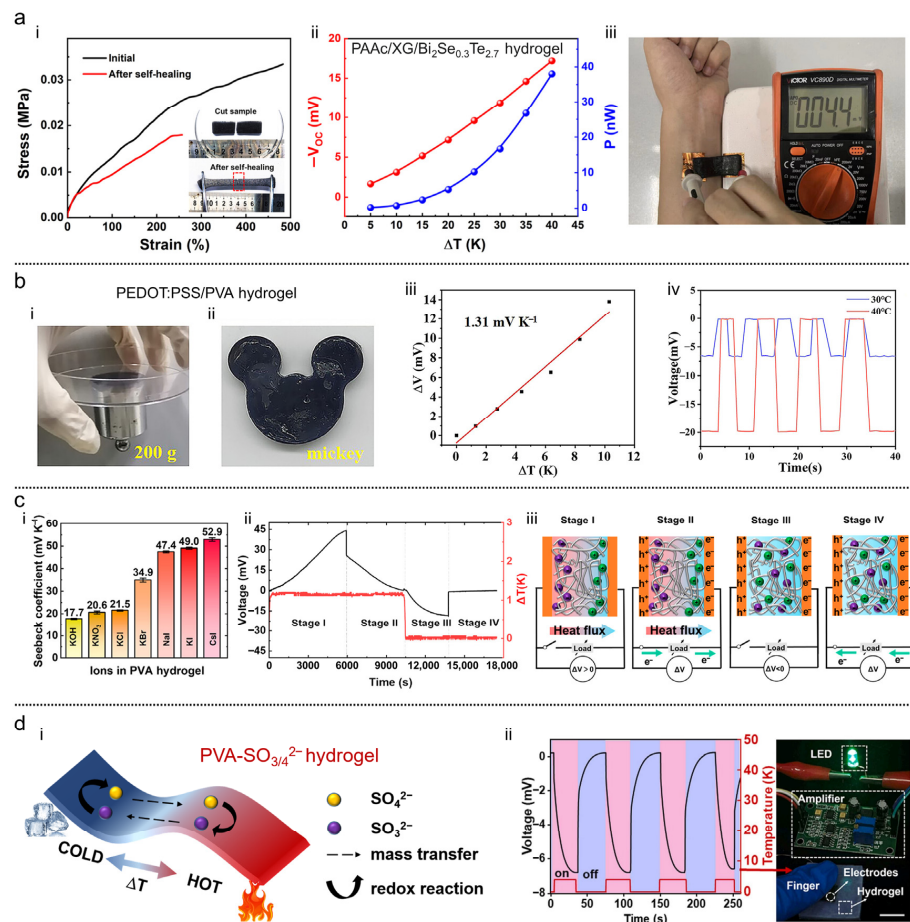


**Figure 5.** (a) Self-healing properties and thermoelectric output performance of the PAAc/XG/Bi<sub>2</sub>Se<sub>0.3</sub>Te<sub>2.7</sub>. (i) Corresponding stress–strain curves for initial and self-healing hydrogels. (ii) Thermoelectric properties of the hydrogel after self-healing. (iii) Output voltage between two ends of the hydrogel.

Reproduced with permission [86]. Copyright 2022, Wiley. (b) Self-adhesive (i), remodeling performance (ii), and thermoelectric properties (iii,iv) of CNC-PEDOT:PSS/PVA hydrogels. Reproduced with permission [87]. Copyright 2023, American Chemical Society. (c) Thermoelectric properties (i) of i-TE materials and operating characteristics (ii,iii) of an i-TE supercapacitor. Reproduced with permission [88]. Copyright 2022, American Chemical Society. (d) Illustration of the operating principle of a TEC based on the thermogalvanic effect (i) and demonstration of the conversion of finger heat into electricity to power an LED (ii). Reproduced with permission [89]. Copyright 2023, Elsevier.

Harnessing the Seebeck effect, the thermoelectric effect enables the direct conversion of heat energy into electrical energy. Poly(3,4-ethylenedioxythiophene):poly(styrene sulfonate) (PEDOT:PSS) is a high-molecular-weight polymer solution consisting of PEDOT doped with anionic PSS, widely recognized for its excellent electrical conductivity. Within the realm of thermoelectric materials, PEDOT:PSS has garnered significant attention for its inherent high electrical conductivity and low thermal conductivity. To expand on this, Chai et al. introduced a novel self-generating hydrogel by incorporating PEDOT:PSS into cellulose nanocrystals (CNCs), as depicted in Figure 5b [87]. This hydrogel showcases outstanding self-healing performance, boasting a remarkable healing efficiency of 92.57%, alongside impressive stretchability, reaching up to 989.60%. Most notably, the hydrogel demonstrates excellent thermoelectric performance, generating stable and reproducible voltages. Additionally, the hydrogel possesses outstanding self-adhesive properties, capable of adhering directly between different substrates, such as plastic and metal, with an adhesion strength of up to 200 g of metal to plastic, providing an adhesion capability that is 100 times its weight (Figure 5b(i)). The exceptional adhesion is primarily attributed to the noncovalent interactions between the hydrogel and diverse substrates, including dynamic hydrogen bonds, metal coordination, and electrostatic interactions. Moreover, the hydrogels can be repeatedly molded into different shapes, such as a mickey shape (Figure 5b(ii)). In terms of thermal-electric performance analysis, the output voltage of the CNC-PEDOT:PSS/PVA hydrogel demonstrates a linear increase with temperature difference, while its Seebeck coefficient measures  $1.31 \text{ mV K}^{-1}$  (Figure 5b(iii)). The hydrogel generates an output voltage of about 6.51 mV at a hot plate temperature of  $30 \text{ }^\circ\text{C}$ , corresponding to a temperature difference ( $\Delta T$ ) of 5 K. By increasing the temperature difference to 15 K, the output voltage can reach 19.68 mV (Figure 5b(iv)). However, removing the device from the hot plate results in a sharp decrease in  $\Delta T$  and subsequently in the output voltage. Once returned to the hot plate, the voltage quickly returns to its original value. The self-powered hydrogel device integrates self-healing, adhesion, and sensing properties, and experimental results demonstrate its ability to effectively convert thermal energy into electrical energy. Adhesion is one of the advantages of hydrogels as a component of wearable devices and helps in adhering the device to the skin surface.

Ionic thermoelectric (i-TE) materials, which utilize movable ions as charge carriers, have demonstrated the ability to generate significant thermal voltages at low operating temperatures. The underlying mechanism of i-TEs is founded on the Soret effect, where a temperature gradient induces an uneven allocation of cations and anions, creating a difference in voltage. To explore the properties of cations and anions in the context of ionic thermoelectrics, He et al. incorporated various inorganic compounds into PVA hydrogels, as shown in Figure 5c [88]. The investigation revealed that the ionic Seebeck coefficient is highly affected by the breaking strength of the anions' structure, as well as the cations. Particularly noteworthy is the Seebeck coefficient of the PVA/CsI hydrogel, which achieves  $52.9 \text{ mV K}^{-1}$  at a 0.1 M concentration (Figure 5c(i)). This is the highlight of the study, which demonstrates remarkably high Seebeck coefficients. Since ions are unable to flow through external circuits, i-TE generators operate by converting heat to electricity in the form of capacitors. The process involves four stages: First, the voltage rises during charging with a temperature gradient (stage I), and the voltage increases. Subsequently, when a load is connected, the charge accrued on the electrode is freed into the external circuit to perform work (stage II). After removing the temperature difference and disconnecting the external circuit, the ions spread back to the initial state (stage III).

Lastly, when the circuit is turned off, the charges on the electrode pass through the load again (stage IV) (Figure 5c(ii,iii)). Apart from their excellent thermoelectric performance, ionic hydrogels also offer advantages such as easy preparation, cost-effectiveness, and mechanical ruggedness. These characteristics suggest that hydrogels with properly selected ions have many advantages in collecting low-grade heat and deserve further exploration for their potential as thermoelectric cells.

Due to the limited flexibility and stretchability of existing materials, significant breakthroughs in self-powered thermoelectric wearables have remained challenging. However, there has been increasing interest in flexible aqueous thermocells using redox couples in the field of wearable electronics. These thermocells offer advantages such as lower production costs and higher thermal–electric conversion efficiency. Numerous studies have focused on the regulation of redox ions and electrolyte solvents to optimize their performance. In a pioneering work by Tian et al., a novel redox couple of  $\text{SO}_4^{2-}/\text{SO}_3^{2-}$  was introduced as a p-type thermogalvanic ion, exhibiting a Seebeck coefficient of  $1.63 \text{ mV K}^{-1}$  when the redox couple concentration was  $0.1 \text{ M}$  [89]. The thermoelectric conversion mechanism is depicted schematically in Figure 5d(i). When the hydrogel is exposed to a temperature gradient, it creates a stable difference in temperature between its two ends, enabling thermopower production by harnessing environmental thermal energy. To demonstrate the potential of collecting low-grade thermal energy, a gel device was connected to an LED through a voltage amplifier with a gain of 357. To enhance safety and minimize risks associated with the gel containing DMSO, it was encapsulated using polyethylene film. The thermoelectric conversion of the device was accomplished by simply touching the film with fingers. When periodically touching the gel with a forefinger, a temperature gradient of approximately  $4 \text{ K}$  was induced, leading to an output voltage value exceeding  $7 \text{ mV}$  (Figure 5d(ii)). This successful demonstration signifies that the heat generated by the finger was effectively converted to power the LED. Redox couple-based thermoelectric conversion mechanism is expected to play an increasingly important role in thermoelectric devices, owing to its good thermoelectric response properties. However, the application demonstration of this work used an amplifier, suggesting that this type of gel requires a further boost in output.

The above-mentioned hydrogel-based thermoelectric devices demonstrated the capability to effectively convert thermal energy into electrical energy by introducing traditional semiconductor thermoelectric materials, conductive polymers, or the Soret effect and the thermogalvanic effect of ions. Additionally, various synergistic effects of thermoelectric phenomena have also been studied to enhance thermoelectric power [90–92].

#### 4.2. Self-Powered Applications of Hydrogel-Based TEG Devices

In this section, we present novel hydrogel-based thermoelectric devices for various applications. A gel electrolyte-based thermogalvanic generator was developed for body temperature monitoring, while a conformal gel-based patch allowed for simultaneous monitoring of body temperature and pulse. A stretchable hydrogel-based thermocell was designed for flexible power generation, and an ultrasensitive flexible thermal sensor array was integrated into a smart glove for object temperature perception. These advancements in hydrogel-based thermoelectric devices provide potential applications in health monitoring, wearable power supply systems, and intelligent interactions.

The first application demonstrated is temperature monitoring. Due to the inherent temperature sensitivity of thermoelectric devices, sensing temperature is also a fundamental self-powered application of thermoelectric devices. Bai et al. presented a gel-based thermogalvanic generator utilizing  $\text{Fe}^{3+}/\text{Fe}^{2+}$  as the redox pair [93]. A mesh-like PVDF diaphragm inserted within the PVA gel was used to fabricate a thermal barrier, effectively enhancing the Seebeck coefficient (Figure 6a). To showcase its potential application in capturing human body heat and detecting vital signs, a gel thermoelectric patch was utilized to establish a body temperature monitoring system, as depicted in Figure 6a(i). The output of the system heavily relies on the temperature difference between the gel's two ends. Consequently, Figure 6a(ii) demonstrates the association between the current

values and body temperature, revealing a steady increase in current with rising temperature across three distinct regions. Remarkably flexible, the gel device can be bent and twisted. Figure 6a(iii) demonstrates that when the gel patch is near a heat source, the current exceeds 80% of its maximal value within 2 s, and declines to 20% within 20 s after moving away from the source. The inset of Figure 6a(iii) shows that the temperature detection limit is 0.1 K. Additionally, when the gel patch is applied to feverish skin, a noticeable temperature reduction is observed, as depicted in Figure 6a(iv), suggesting a significant cooling effect provided by the gel. Furthermore, as a gel patch, water retention is a crucial consideration. With its rapid response/recovery, low detection limit, and cyclic stability to temperature differences, the gel patch-based wearable sensor proves to be an effective tool for monitoring human temperature.

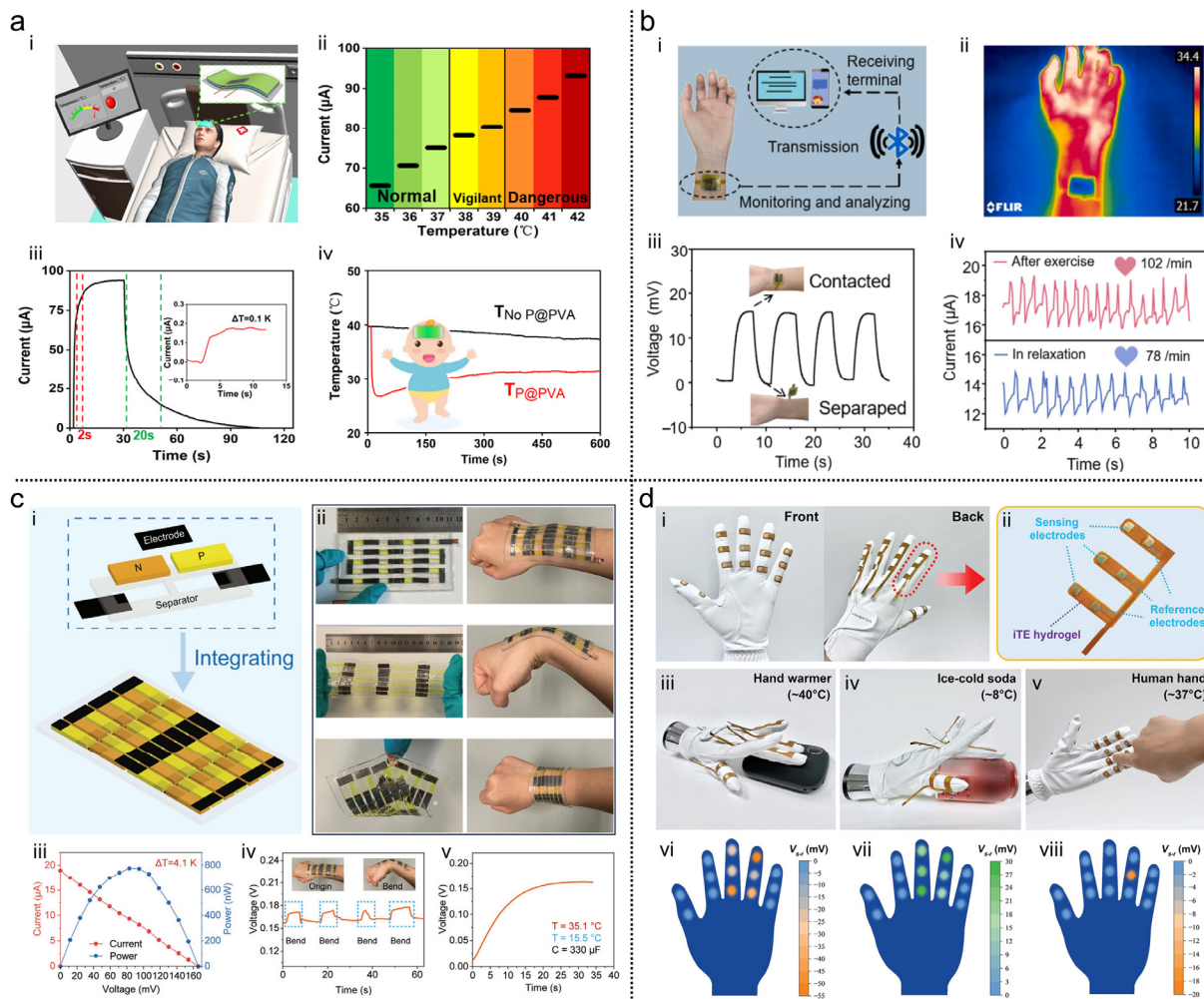


**Figure 6.** (a) Application demonstration of thermogalvanic gel-based wearable body temperature detection. (i) Schematic illustration of the use of a gel patch for body temperature monitoring. (ii) Correlation between current and body temperature. (iii) Current response curve as well as an inset showing the current profile at a 0.1 K temperature difference. (iv) Cooling effect of the gel when affixed to the skin. Reproduced with permission [93]. Copyright 2021, American Chemical Society. (b) Applications of the body temperature detection and pulse responder. (i) Workflow schematic of the body temperature and pulse measurement. (ii) Infrared image of a gel patch attached to a wrist. (iii) Output voltage profile during repeated contact and separation cycles between the gel and the wrist. (iv) Current versus time while monitoring the wrist pulse of a volunteer at rest and after exercise. Reproduced with permission [94]. Copyright 2023, Elsevier. (c) Hydrogel thermocell for thermal energy harvesting. (i) Illustration depicting the integration. (ii) Photos capturing the thermo-

cell device affixed to the body in various deformation modes. (iii) Thermoelectric performance of a device incorporating 14 pairs of p-n cells. (iv) Voltage–time plot of the thermocell attached to the wrist. (v) Voltage–time curve of a capacitor charged by the thermocell. Reproduced with permission [95]. Copyright 2022, Wiley. (d) Smart glove with spatial heat perception. (i) Smart glove with integrated thermal sensor arrays. (ii) Thermal sensor array affixed to each finger. Demonstrating the thermal sensory function of the glove when touching (iii,vi) a warmer, (iv,vii) a soda can, and (v,viii) a hand. Reproduced with permission [96]. Copyright 2023, Wiley.

In addition to temperature measurement, there are studies showing the usage of pulse detection. Zhang et al. developed a conformal TEG utilizing  $\text{Fe}^{2+}/\text{Fe}^{3+}$  electrolyte-based hydrogels and multi-walled carbon nanotube (MWCNT) electrodes [94]. Leveraging its exceptional thermoelectric performance, flexibility, and stretchability, a self-powered health monitoring patch capable of conformally attaching to the wrist or other areas was fabricated (Figure 6b). This thermogalvanic gel-based patch enables simultaneous monitoring of vital physiological signals, including pulse and body temperature, when placed on the wrist area. As depicted in Figure 6b(i), the sensing signals are acquired using a cell phone terminal for quantitative analysis. Due to the permanent temperature gap between the human body and the surrounding air, where the air temperature remains nearly constant, the foundation for testing temperature is established. Figure 6b(ii) illustrates an infrared image of the hydrogel patch adhered to the wrist. Figure 6b(iii) showcases the voltage signal profiles as the hydrogel contacts and leaves the skin, demonstrating the ideal cycling characteristics of the thermoelectric gel. Additionally, the gel can monitor changes in the volunteer's wrist pulse rate, as shown in Figure 6b(iv), detecting a rate of 78 beats per minute (bpm) while relaxed and 102 bpm after exercise. This research holds significant implications in disease detection and health care, providing new insights for the development of self-powered epidermal medical wearables.

While the above two studies only demonstrate the use of a single gel, the following study illustrates the integration of multiple hydrogel units with different thermoelectric properties to multiply the output. Xu et al. used a PAAm-based super-stretchable hydrogel as an excellent substrate for thermocells, enabling adaptation to body surfaces.  $\text{Fe}(\text{ClO}_4)_3/\text{Fe}(\text{ClO}_4)_2$  was chosen as the n-type ion pair due to its comparable thermoelectric properties to  $\text{K}_3[\text{Fe}(\text{CN})_6]/\text{K}_4[\text{Fe}(\text{CN})_6]$  (p-type elements) [95]. By integrating inherently stretchable hydrogels and graphite paper electrodes, a body-conformable thermocell was prepared using a traditional  $\pi$ -like device structure (Figure 6c). Unlike parallel electrodes, staggered electrodes were used in this design to provide a stretchable area for device deformation. This electrode configuration, combined with the hydrogel's excellent adhesion, prevented relative shifting between the electrodes and hydrogel under lateral forces. Using the aforementioned design concept, 14 p-n pairs of hydrogel elements were integrated into a thermocell sheet (Figure 6c(i)). As illustrated in Figure 6c(ii), the thermocell effectively adhered to curved body surfaces such as arm and wrist joints, adapting well to deformations. At a temperature drop of 4.1 K, the thermocell achieved an output voltage of 160 mV and a maximal power of 0.77  $\mu\text{W}$  (Figure 6c(iii)). Notably, the voltage slightly increased as the wrist joint deformed from 0° to 90°, facilitating better contact with the human body (Figure 6c(iv)). Furthermore, the wearable thermocell was capable of charging a 330  $\mu\text{F}$  capacitor (Figure 6c(v)). This work demonstrated the potential of thermogalvanic cells for applications in everyday power supply systems, offering advantages such as low cost, decent output behavior, simple structure, and skin-like appearances.

Likewise using multiple gel units, Han et al. presented an ultrasensitive thermal sensor array based on an ionic thermoelectric hydrogel composed of polyquaternium-10 (PQ-10) and NaOH as the ion source [96]. The developed PQ-10/NaOH hydrogel reaches a high Seebeck coefficient of 24.17  $\text{mV K}^{-1}$ . To showcase the application in artificial sensing, a smart glove that integrates PQ-10/NaOH sensors was fabricated (Figure 6d). Emulating the thermal feeling of human skin, 14 nodes were strategically located on the five fingers of the glove (Figure 6d(i)). Each finger was equipped with an array of thermal sensors, with the sensing and reference electrodes attached to the anterior and posterior sides of the finger

(Figure 6d(ii)). The glove was then put on a fake hand and tested by touching different temperature objects (Figure 6d(iii–v)). The corresponding voltages of the smart glove contacted with a warmer ( $\approx 40^\circ\text{C}$ ), a soda can ( $\approx 8^\circ\text{C}$ ), and a hand ( $\approx 37^\circ\text{C}$ ) are depicted in (Figure 6d(vi–viii)). Upon contact with a hot or cold object, the sensing nodes touching the object recorded negative or positive voltages, while the voltages for other sensing nodes remained near zero. By detecting the voltages of all sensor nodes, the smart glove is capable of perceiving the temperature and touch position of an object, demonstrating the promising application for intelligent robot–environment interaction.

The excellent thermal–electric conversion performance, flexibility, conformability, and biocompatibility of hydrogel enable it to adapt to various wearable scenarios, expanding the application range of traditional self-powered devices based on thermoelectric effects. Furthermore, combining the thermoelectric effect with other effects can give rise to more sensing strategies. In the following section, self-powered sensing applications based on various effects (including the aforementioned triboelectric effect, piezoelectric effect, and thermoelectric effect) will be demonstrated.

## 5. Energy Harvesters and Self-Powered Wearable Applications Based on Hybrid Effects

### 5.1. Triboelectric, Piezoelectric, and Piezoresistive Effects

With the continuous improvement of wearable devices, nanogenerator technology with self-powered sensing potential has received significant attention in recent years. The piezoelectric effect and triboelectric effect are commonly used mechanisms in human motion sensing. Self-powered devices based on these two effects generally exhibit improved output performance compared with single-type devices [97–100]. Furthermore, the piezoresistive effect typically refers to the phenomenon where the resistance of a semiconductor changes due to the variation in energy levels of the conduction band caused by stress-induced band structure changes [101–104]. However, in the context of hydrogel applications, the piezoresistive effect generally refers to changes in resistance resulting from variations in the dimensions of the gel under deformation [105–108]. Based on this characteristic, hydrogels can be used for stress or strain sensing.

Wang et al. developed a flexible and highly transparent PAM/BTO ( $\text{BaTiO}_3$  nanocubes) complex hydrogel in a self-powered sensor, using the synergistic effects of piezoelectric, triboelectric, and piezoresistive properties [109]. The hydrogel film could be used directly as a piezoresistive sensor. A sandwich-structured TENG working in single-electrode mode was prepared while hydrogels served as electrodes, with a PTFE film as the triboelectric layer and an acrylic board as the support (Figure 7a). The working mechanism of the TENG is rooted in the combined effects of the triboelectric and piezoelectric properties of the BTO-containing hydrogel. The PAM/BTO hydrogels demonstrated improved TENG performance compared with pure hydrogels, attributed to the positive influence of BTO on the output (Figure 7b). Finite-element simulation using COMSOL elucidated the proposed mechanism, further confirming the enhancement resulting from the piezoelectric charges induced by the BTO nanotubes (Figure 7c,d).

By leveraging the hydrogel-based TENG sensor, it was possible to monitor small pressures, accurately determine weights, and recognize walking postures in real time. The sensor successfully sensed finger sliding on a mobile phone surface and knee movements by measuring  $V_{oc}$  between the human body and the ground (Figure 7e,f). With the composite hydrogel sensor on the heel, different weights of student volunteers were distinguished based on the sensitivity of the sensor, while the distinct frequencies of voltage pulses reflected the habits of different volunteers (Figure 7g). Consequently, the hydrogel-based TENG exhibited promising applications in gait detection and weight measurement, which are scenarios that include pressing action.

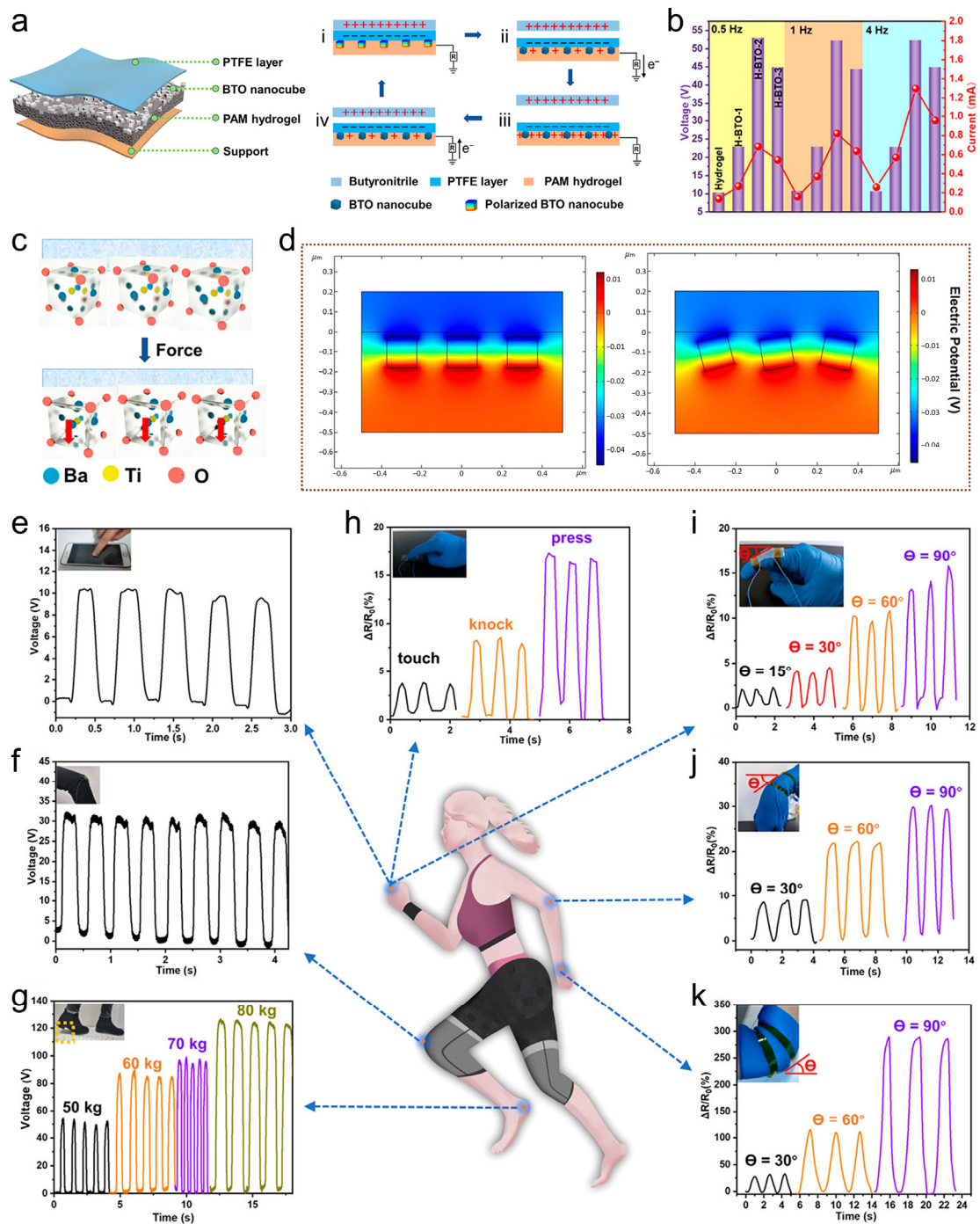


**Figure 7.** (a) Schematic diagrams and (i–iv) operating principle of the sandwich-like TENG. (b) Comparison of voltage and current outputs between TENGs with pure hydrogel and PAM/BTO hydrogels. (c) Schematic diagram illustrating the production of piezoelectric charges in BTO. (d) Finite-element simulation depicting the potential distribution in BTO composite hydrogel for BTO nanoparticles with different distributions under a loaded force of 1 N. (e) Voltage output of the self-powered TENG sensor for detecting pressure on a mobile phone. (f) TENG sensor attached to the knee. (g) TENG sensor (highlighted with a yellow box) attached at the heel, distinguishing different weights. (h–k)  $\Delta R/R_0$  values for the hydrogel piezoresistive sensor detecting (h) different contact strengths, (i) finger bending, (j) wrist motion, and (k) elbow bending. Reproduced with permission [109]. Copyright 2022, American Chemical Society.

Additionally, the good stretchability of hydrogels was exploited to use them directly as pressure and curvature sensors. The hydrogel-based piezoresistive sensor was mounted on a variety of joint-containing parts for sensing sophisticated motion changes. The resistance change in the hydrogel, resulting from the variation in the cross-sectional area during sensor deformation, converted strain signals into electric signals, allowing for the detection of finger touch, tapping, and pressing with high sensitivity (Figure 7h). Furthermore, the hydrogel-based sensor sensitively detected finger bending at various angles (15, 45, 60, and 90°), as recorded in Figure 7i. As the bending angle increased from 0 to 90°, a gradual increase in  $\Delta R/R_0$  (change in resistance) was observed due to increased sensor stretching. The sensor also accurately monitored the large motion of the wrist and elbow, evidenced by the step increase in  $\Delta R/R_0$  corresponding to the elbow bending angle (Figure 7j,k). The sensor demonstrated the ability to distinguish pressure and sense both minor and major movements during exercise.

In summary, the PAM/BTO hydrogel-based sensors exhibited high sensitivity, accuracy, and repeatability. The study demonstrates the enormous potential of hydrogel devices that combine triboelectric, piezoelectric, and piezoresistive effects for real-time biomechanical sensing applications.

### 5.2. Photothermal and Thermoelectric Effects

Solar energy is a green source of energy that is abundant and inexhaustible. Given the challenges posed by climate change and the energy crisis, the conversion of solar energy into other forms of energy has gained significant research interest [110]. Photothermal materials are a class of materials that convert absorbed light energy into heat and have significant potential application prospects in solar thermal conversion [111]. Various photothermal materials have been studied, such as MoS<sub>2</sub> [112], CuS [113], Fe<sub>3</sub>O<sub>4</sub> [114], and gold nanoparticles [115], among others. The following study demonstrates a strategy for photo-thermal-electric (PTE) conversion using a combination of photothermal materials and the thermoelectric effect of hydrogels.

In a recent study, Yang et al. present a PTE hydrogel for human motion detection [116]. The design leverages the low thermal conductivity and high output power of PVA-PDMS gels, while Fe<sup>2+/3+</sup> is selected as the redox pair. The key to achieving photothermal conversion in their study is the utilization of the local surface plasmon resonance (LSPR) of Au nanoparticles (AuNPs). This enables simultaneous high thermoelectric and photothermal performance. A schematic diagram of the PTE device is depicted in Figure 8a, consisting of a photothermal layer, a thermoelectric hydrogel, and carbon paper serving as the current collectors at the two ends of the hydrogel. To enhance solar-thermal conversion performance, AuNPs@SiO<sub>2</sub> are embedded within the PDMS, with SiO<sub>2</sub> nanoparticles playing a crucial role in increasing the light scattering and dispersing the AuNPs, resulting in improved light absorption and photothermal conversion. The significant quantity of AuNPs@SiO<sub>2</sub> incorporated contributes to the enhanced photothermal conversion ability of the composites. The PDMS layer is transparent, facilitating easy photon access to the surface of AuNPs@SiO<sub>2</sub>. Based on the LSPR effect, AuNPs undergo a plasma-enhanced photothermal effect when exposed to a resonant wavelength.

Figure 8b illustrates a schematic diagram of the PTE patch designed for human motion sensing. During the thermogalvanic conversion process, the exposure of the patch to external sunlight is influenced by the arm swing, which in turn causes the temperature of the gel to change. The detected output current primarily depends on variations in solar light intensity incident on the patch. The solar-actuated gel exhibits a larger temperature variation with increasing light strength, as demonstrated in Figure 8c, supported by the top and side infrared pictures of the PTE device in Figure 8d. The gel sensor has quick responses and distinguishable current signals, proving that it can effectively detect human motion (Figure 8e). Different arm swing frequencies typically indicate varying speeds of body movements. The current plots verify that the current amplitude is correlated with the arm swing frequency (Figure 8f). A higher frequency results in a shorter rising time for the

current, leading to a decrease in current amplitude. The current waves created by the gel patch can be transferred to the cell phone terminal, enabling the detection and recognition of common human body movements (Figure 8g).

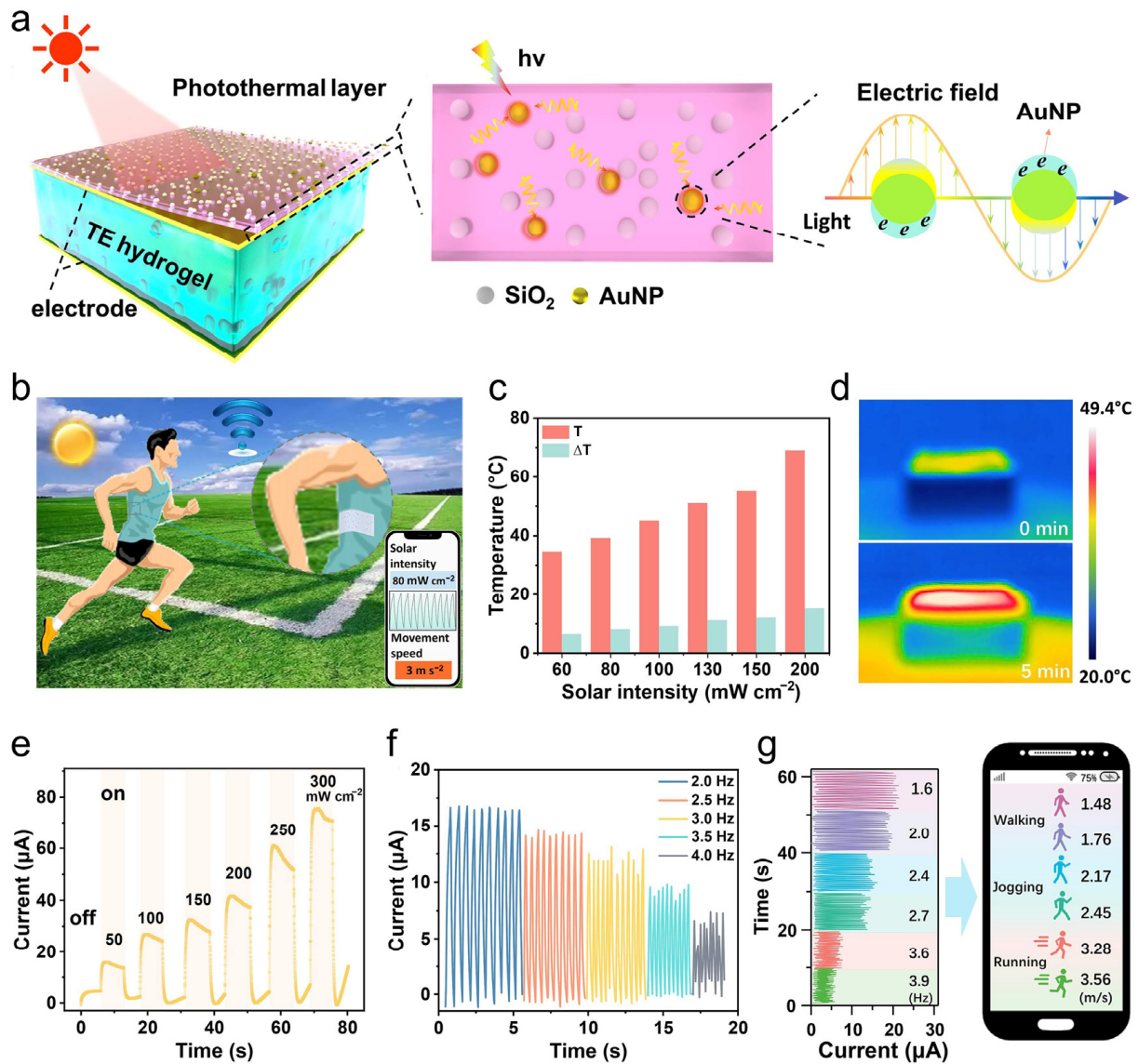


**Figure 8.** (a) Schematic representation of the designed Photo-Thermal-Electrochemical (PTE) device for thermal sensing. (b) Schematic of the PTE patch used for human movement detection. (c) Variation in the photothermal layer's temperature and temperature differences. (d) Infrared pictures of the photothermal layer. (e) Current variations at different sunlight levels. (f) Changes in current at different swing arm rates. (g) Recognition of key movement patterns, such as walking, jogging, and running. Reproduced with permission [116]. Copyright 2023, Elsevier.

This work presents a PTE patch that not only enables non-contact control but also has the potential to be integrated with therapeutic devices for adaptive regulation of human physiological states. Additionally, previous studies have showcased the versatility of PTE conversion, which not only facilitates power generation but also finds applications in freshwater production and light intensity monitoring [117–119]. In conclusion, these PTE devices offer a novel avenue for harnessing solar energy and transforming it into electrical energy.

### 5.3. Thermoelectric and Piezoresistive Effects

Thermoelectric hydrogel materials encompass both thermoelectric and piezoresistive effects. Previous studies have shown elastomer sensors capable of dual-mode sensing for temperature and pressure [120–122]. The following section presents a demonstration of hydrogel devices based on both effects for detecting temperature and pressure.

Fu et al. presented a stretchable and self-powered dual-sensing i-skin based on thermogalvanic hydrogels (TGHs) for simultaneous detection of temperature and pressure [123]. The TGH sensor was fabricated by incorporating the redox couple  $K_4Fe(CN)_6/K_3Fe(CN)_6$  into PAM hydrogels and further sandwiched by two titanium foil electrodes. Leveraging both the piezoresistive and thermogalvanic effect of the hydrogel, temperature and pressure excitations can be turned into voltage and current responses, enabling the perception of the variables at the same time.

The mechanism of sensing is illustrated in Figure 9a. When an external temperature stimulus is applied to the TGH sensor, a temperature difference is formed between the electrodes, leading to a potential difference across the hydrogel due to the reversible reaction of the redox couple. A TGH sensor immobilized on a thermostatic substrate can immediately sense the surface temperature. Additionally, the internal resistance of the TGH sensor changes with shape deformation caused by external pressure stimuli (Figure 9b), allowing pressure to be perceived by monitoring the current variation. When both temperature and pressure stimuli are presented, the voltage output and current variation can be tested by monitoring the voltage and relative voltage change in the resistance connected to the hydrogel, respectively. This is how the TGH sensor works to detect both temperature and pressure stimulation. Specifically, when only a temperature stimulus is applied, the slope of the resistance profile remains unchanged, demonstrating that the temperature change has a negligible effect on the resistance (Figure 9c). The effective internal resistance of the TGH is influenced by the hydrogel thickness. It is evident from the I–V plots that the  $V_{oc}$  of the sensor remains unaltered at different pressures, affirming that external pressure stimuli do not affect the output voltage (Figure 9d). Consequently, TGH sensors can detect both pressure and temperature at the same time without interference.

To fulfill the requirements for practical applications, a TGH array was designed for space sensing. Figure 9e illustrates the detailed structure of the sensor array. The TGH was packaged by Ecoflex, with a snake-like electrode array for spatial temperature–pressure sensing. This structure ensures uniform strain distribution when stretching occurs (Figure 9f). In response to gentle finger pressure on one of the pixels ( $P_1$ ), stable voltage and current responses were observed during consecutive loading–unloading loops, while the neighboring pixel ( $P_2$ ) did not have any reaction (Figure 9g), confirming that the pixels can perform space sensing without interference.

The strain-tolerant and space temperature–pressure monitoring abilities of the fabricated sensor array were demonstrated in two cases. In the first case, the stretchable array was used to digitally monitor tactile messages of human skin, unaffected by limb motions. A TGH sensor array was attached to the back of the wrist to gauge a variety of external tactile signals. Figure 9h depicts apparent stretching of the TGH device caused by wrist bending, while quantifiable stimuli were identified when objects of different temperatures or masses were touched by the flexible array, regardless of stretching (Figure 9i,j). In the second demonstration, a weight was placed on the TGH array to showcase its space temperature–pressure monitoring characteristics (Figure 9k). The space tactile messages captured by the stretchable array align with the locations of the applied weight (Figure 9l,m). The proposed design exhibits strain-tolerant and space-perception capabilities, holding promise for applications in artificial intelligence, human–computer interaction, and virtual reality.

The strategy demonstrated above, which combines multiple effects to achieve self-powered sensing applications, not only expands the ways of power generation but also unlocks a plethora of usage scenarios, paving the way for further developments in wearable electronics. This approach opens up a range of possibilities for wearable applications, contributing to the overall development of wearable electronics.

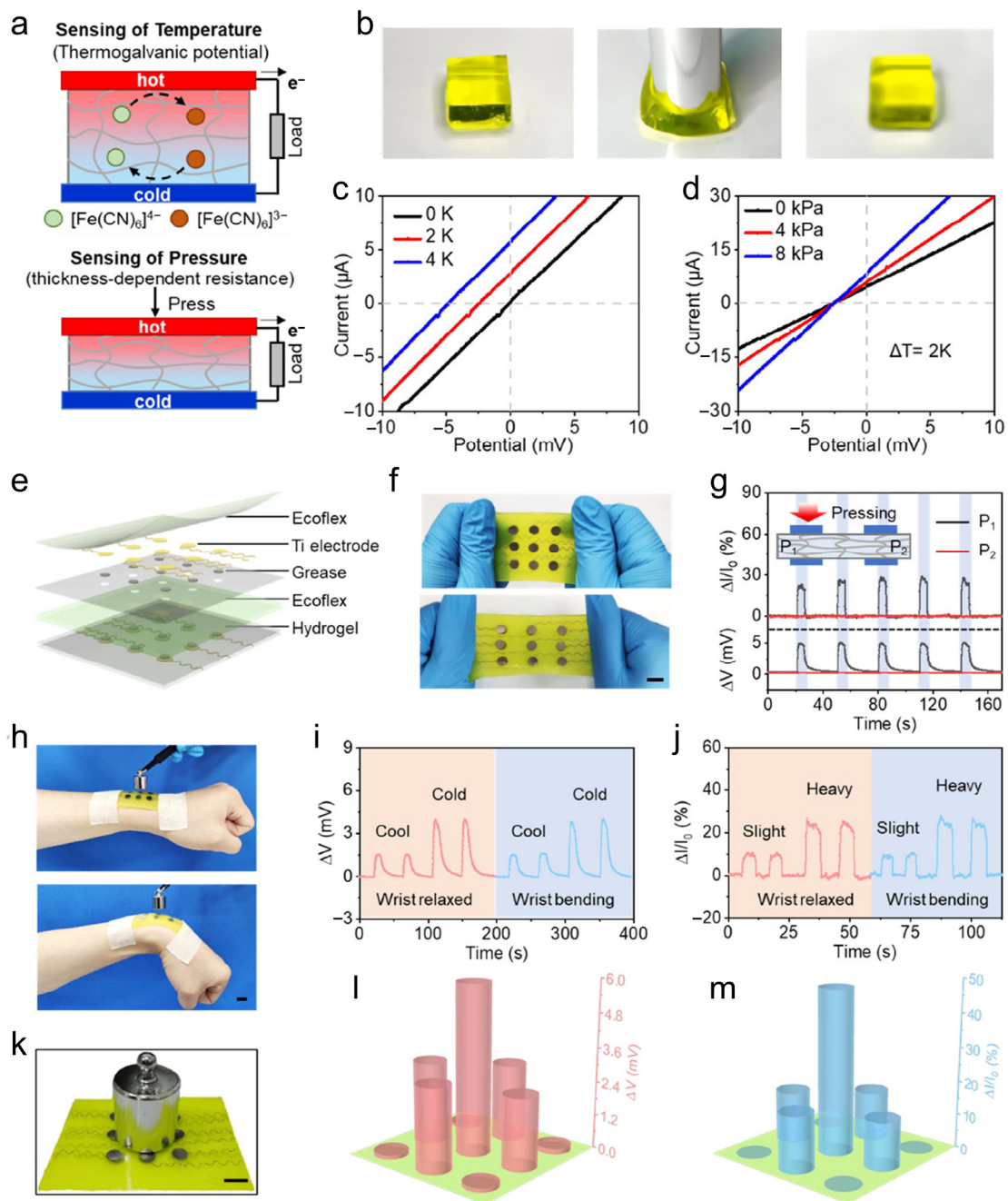


**Figure 9.** (a) Principle of monitoring temperature and pressure. (b) Compressing ability of TGH hydrogels. (c,d) I–V plots under different  $\Delta T$  (c) and loading pressures (d). (e) Schematic diagram of the sensor array. (f) The TGH sensor array’s tensile characteristics. (g) Results of thermal voltage output and current variation. (h) Photos of the TGH array on the wrist in the comfortable and bent position. Voltage (i) and current shift (j) when items with various temperatures and pressures are applied. (k) Schematic diagram illustrating simultaneous detection of pressure and temperature. Voltage (l) and current variation (m) in the array in (k). All scales are 10 mm. Reproduced with permission [123]. Copyright 2022, American Chemical Society.

### 6. Conclusions and Outlook

Given the numerous advantages of hydrogels, such as conductivity, high sensitivity, flexibility, mechanical strength, self-healing, and biocompatibility, the integration of hydrogels with energy harvesting devices (TEGs, PENGs, TENGs) expands the possibilities of self-powered applications, particularly in wearable devices. This study reviews the litera-

ture and latest developments in energy harvesters based on hydrogels, including device construction and their self-powered sensing applications in wearable scenarios. Moreover, the achievements of hybrid devices based on various energy harvesting strategies are highlighted.

To accelerate the incorporation of hydrogels into flexible wearable electronic devices, it is recommended to take the following measures and overcome related challenges. Firstly, from the material aspect, lots of progress has been made in current research to obtain materials such as self-adhesive, self-healing, and durable properties by modulating the mechanical/electrical properties of hydrogels. However, in the design process of hydrogel-based generators, the mechanical strength of other parts of the devices should be considered to prolong their lifespan in scenarios where they are subject to frequent external forces, such as joint bending. Alternatively, packaging or integration processes can be used to enhance the overall stability of the device's output. For energy harvesting, attention should be paid to improving the output power density of energy conversion devices. The process of practical application of various energy harvesters can be promoted with more effective means. For example, energy management strategies can be applied to hydrogel-based TENGs to make them better adapt to self-powered demand. Additionally, while hydrogels offer flexibility and ease of conformability, which make them well-suited for wearable applications, most of the research on hydrogel sensors has been conducted with wired connections. However, it is not suitable to have multiple exposed wires in wearable applications, which limits their adoption in commercial electronic devices. The future application of hydrogels can be combined with wireless information transmission technology to expand the functionality of hydrogel devices in a convenient and wireless direction. Another significant issue with self-powered sensors is that sensing demonstrations should not only focus on simple functionality but also the technical parameters and comparisons with commercial sensors. Some technical parameters should be proposed for different types of self-powered sensors to standardize the performance specifications of the tested devices.

**Author Contributions:** Conceptualization, Z.W. and H.Z.; writing—original draft preparation, Z.W.; review and editing, N.L., Z.Z. and X.C.; funding acquisition, H.Z. All authors have read and agreed to the published version of this manuscript.

**Funding:** This work was supported by the Natural Science Foundation of Shanxi Province (20210302123190) and the Special Project of Science and Technology Cooperation and Exchange of Shanxi Province (202104041101031).

**Data Availability Statement:** No new data were created or analyzed in this study. Data sharing is not applicable to this article.

**Conflicts of Interest:** The authors declare no conflict of interest.

## References

1. Lin, J.; Zhu, Z.; Cheung, C.F.; Yan, F.; Li, G. Digital manufacturing of functional materials for wearable electronics. *J. Mater. Chem. C* **2020**, *8*, 10587–10603. [[CrossRef](#)]
2. Xu, K.; Lu, Y.; Takei, K. Multifunctional Skin-Inspired Flexible Sensor Systems for Wearable Electronics. *Adv. Mater. Technol.* **2019**, *4*, 1800628. [[CrossRef](#)]
3. Xu, X.; Zhao, Y.; Liu, Y. Wearable Electronics Based on Stretchable Organic Semiconductors. *Small* **2023**, *19*, 2206309. [[CrossRef](#)] [[PubMed](#)]
4. Zhu, C.; Wu, J.; Yan, J.; Liu, X. Advanced Fiber Materials for Wearable Electronics. *Adv. Fiber Mater.* **2023**, *5*, 12–35. [[CrossRef](#)]
5. Lee, J.-H.; Yang, G.; Kim, C.-H.; Mahajan, R.L.; Lee, S.-Y.; Park, S.-J. Flexible solid-state hybrid supercapacitors for the internet of everything (IoE). *Energy Environ. Sci.* **2022**, *15*, 2233–2258. [[CrossRef](#)]
6. Wang, L.; Zhang, Y.; Pan, J.; Peng, H. Stretchable lithium-air batteries for wearable electronics. *J. Mater. Chem. A* **2016**, *4*, 13419–13424. [[CrossRef](#)]
7. Wu, Z.; Wang, Y.; Liu, X.; Lv, C.; Li, Y.; Wei, D.; Liu, Z. Carbon-Nanomaterial-Based Flexible Batteries for Wearable Electronics. *Adv. Mater.* **2019**, *31*, 1800716. [[CrossRef](#)]
8. Zhang, P.; Wang, F.; Yu, M.; Zhuang, X.; Feng, X. Two-dimensional materials for miniaturized energy storage devices: From individual devices to smart integrated systems. *Chem. Soc. Rev.* **2018**, *47*, 7426–7451. [[CrossRef](#)]

9. Chen, J.; Guo, H.; Pu, X.; Wang, X.; Xi, Y.; Hu, C. Traditional weaving craft for one-piece self-charging power textile for wearable electronics. *Nano Energy* **2018**, *50*, 536–543. [[CrossRef](#)]
10. Guo, H.; Yeh, M.-H.; Lai, Y.-C.; Zi, Y.; Wu, C.; Wen, Z.; Hu, C.; Wang, Z.L. All-in-One Shape-Adaptive Self-Charging Power Package for Wearable Electronics. *ACS Nano* **2016**, *10*, 10580–10588. [[CrossRef](#)]
11. Li, S.; Wang, J.; Peng, W.; Lin, L.; Zi, Y.; Wang, S.; Zhang, G.; Wang, Z.L. Sustainable Energy Source for Wearable Electronics Based on Multilayer Elastomeric Triboelectric Nanogenerators. *Adv. Energy Mater.* **2017**, *7*, 1602832. [[CrossRef](#)]
12. Teixeira, J.S.; Costa, R.S.; Pires, A.L.; Pereira, A.M.; Pereira, C. Hybrid dual-function thermal energy harvesting and storage technologies: Towards self-chargeable flexible/wearable devices. *Dalton Trans.* **2021**, *50*, 9983–10013. [[CrossRef](#)] [[PubMed](#)]
13. Wang, X.; Xiao, Y.; Deng, F.; Chen, Y.; Zhang, H. Eye-Movement-Controlled Wheelchair Based on Flexible Hydrogel Biosensor and WT-SVM. *Biosensors* **2021**, *11*, 198. [[CrossRef](#)] [[PubMed](#)]
14. Zheng, H.; Lin, N.; He, Y.; Zuo, B. Self-Healing, Self-Adhesive Silk Fibroin Conductive Hydrogel as a Flexible Strain Sensor. *ACS Appl. Mater. Interfaces* **2021**, *13*, 40013–40031. [[CrossRef](#)] [[PubMed](#)]
15. Feng, Y.; Yu, J.; Sun, D.; Dang, C.; Ren, W.; Shao, C.; Sun, R. Extreme environment-adaptable and fast self-healable eutectogel triboelectric nanogenerator for energy harvesting and self-powered sensing. *Nano Energy* **2022**, *98*, 107284. [[CrossRef](#)]
16. Li, G.; Li, L.; Zhang, P.; Chang, C.; Xu, F.; Pu, X. Ultra-stretchable and healable hydrogel-based triboelectric nanogenerators for energy harvesting and self-powered sensing. *RSC Adv.* **2021**, *11*, 17437–17444. [[CrossRef](#)]
17. Vijayakanth, T.; Shankar, S.; Finkelstein-Zuta, G.; Rencus-Lazar, S.; Gilead, S.; Gazit, E. Perspectives on recent advancements in energy harvesting, sensing and bio-medical applications of piezoelectric gels. *Chem. Soc. Rev.* **2023**, *52*, 6191–6220. [[CrossRef](#)]
18. Kong, S.; Huang, Z.; Hu, Y.; Jiang, Y.; Lu, Y.; Zhao, W.; Shi, Q.; Yuan, M.; Dai, B.; Li, J.; et al. Tellurium-nanowire-doped thermoelectric hydrogel with high stretchability and seebeck coefficient for low-grade heat energy harvesting. *Nano Energy* **2023**, *115*, 108708. [[CrossRef](#)]
19. Liu, Z.; Wang, X.; Wei, S.; Lv, H.; Zhou, J.; Peng, P.; Wang, H.; Chen, G. A Wavy-Structured Highly Stretchable Thermoelectric Generator with Stable Energy Output and Self-Rescuing Capability. *CCS Chem.* **2021**, *3*, 2404–2414. [[CrossRef](#)]
20. Pan, S.; Zhang, Z. Fundamental theories and basic principles of triboelectric effect: A review. *Friction* **2019**, *7*, 2–17. [[CrossRef](#)]
21. Kim, K.N.; Lee, J.P.; Lee, S.H.; Lee, S.C.; Baik, J.M. Ergonomically designed replaceable and multifunctional triboelectric nanogenerator for a uniform contact. *RSC Adv.* **2016**, *6*, 88526–88530. [[CrossRef](#)]
22. Rana, S.M.S.; Rahman, M.T.; Sharma, S.; Salaudin, M.; Yoon, S.H.; Park, C.; Maharjan, P.; Bhatta, T.; Park, J.Y. Cation functionalized nylon composite nanofibrous mat as a highly positive friction layer for robust, high output triboelectric nanogenerators and self-powered sensors. *Nano Energy* **2021**, *88*, 106300. [[CrossRef](#)]
23. Li, S.; Peng, W.; Wang, J.; Lin, L.; Zi, Y.; Zhang, G.; Wang, Z.L. All-Elastomer-Based Triboelectric Nanogenerator as a Keyboard Cover To Harvest Typing Energy. *ACS Nano* **2016**, *10*, 7973–7981. [[CrossRef](#)] [[PubMed](#)]
24. Hu, D.; Yao, M.; Fan, Y.; Ma, C.; Fan, M.; Liu, M. Strategies to achieve high performance piezoelectric nanogenerators. *Nano Energy* **2019**, *55*, 288–304. [[CrossRef](#)]
25. Deng, W.; Zhou, Y.; Libanori, A.; Chen, G.; Yang, W.; Chen, J. Piezoelectric nanogenerators for personalized healthcare. *Chem. Soc. Rev.* **2022**, *51*, 3380–3435. [[CrossRef](#)]
26. Pei, H.; Jing, J.; Chen, Y.; Guo, J.; Chen, N. 3D printing of PVDF-based piezoelectric nanogenerator from programmable metamaterial design: Promising strategy for flexible electronic skin. *Nano Energy* **2023**, *109*, 108303. [[CrossRef](#)]
27. Zhou, Y.-X.; Lin, Y.-T.; Huang, S.-M.; Chen, G.-T.; Chen, S.-W.; Wu, H.-S.; Ni, I.C.; Pan, W.-P.; Tsai, M.-L.; Wu, C.-I.; et al. Tungsten disulfide nanosheets for piezoelectric nanogenerator and human-machine interface applications. *Nano Energy* **2022**, *97*, 107172. [[CrossRef](#)]
28. Tohidi, F.; Ghazanfari Holagh, S.; Chitsaz, A. Thermoelectric Generators: A comprehensive review of characteristics and applications. *Appl. Therm. Eng.* **2022**, *201*, 117793. [[CrossRef](#)]
29. Tabaie, Z.; Omidvar, A. Human body heat-driven thermoelectric generators as a sustainable power supply for wearable electronic devices: Recent advances, challenges, and future perspectives. *Heliyon* **2023**, *9*, e14707. [[CrossRef](#)]
30. Shi, Y.; Wang, Y.; Deng, Y.; Gao, H.; Lin, Z.; Zhu, W.; Ye, H. A novel self-powered wireless temperature sensor based on thermoelectric generators. *Energy Convers. Manag.* **2014**, *80*, 110–116. [[CrossRef](#)]
31. Hassanzadeh, A.; Baghestani, S. A New Self-Powered Temperature Sensor Based on Thermoelectric Generators. *IEEE Sens. J.* **2022**, *22*, 22421–22427. [[CrossRef](#)]
32. Wu, S.; Dong, P.; Cui, X.; Zhang, Y. The strategy of circuit design for high performance nanogenerator based self-powered heart rate monitor system. *Nano Energy* **2022**, *96*, 107136. [[CrossRef](#)]
33. Su, Y.; Chen, G.; Chen, C.; Gong, Q.; Xie, G.; Yao, M.; Tai, H.; Jiang, Y.; Chen, J. Self-Powered Respiration Monitoring Enabled By a Triboelectric Nanogenerator. *Adv. Mater.* **2021**, *33*, 2101262. [[CrossRef](#)] [[PubMed](#)]
34. Jiang, Y.; Zhang, Y.; Ning, C.; Ji, Q.; Peng, X.; Dong, K.; Wang, Z.L. Ultrathin Eardrum-Inspired Self-Powered Acoustic Sensor for Vocal Synchronization Recognition with the Assistance of Machine Learning. *Small* **2022**, *18*, 2106960. [[CrossRef](#)] [[PubMed](#)]
35. Si, J.; Duan, R.; Zhang, M.; Liu, X. Recent Progress Regarding Materials and Structures of Triboelectric Nanogenerators for AR and VR. *Nanomaterials* **2022**, *12*, 1385. [[CrossRef](#)]
36. Qiao, W.; Zhou, L.; Zhao, Z.; Liu, D.; Li, S.; An, J.; Li, X.; Gao, Y.; Yang, P.; Liu, J.; et al. A self-powered vector motion sensor for smart robotics and personalized medical rehabilitation. *Nano Energy* **2022**, *104*, 107936. [[CrossRef](#)]

37. Sahoo, S.; Krishnamoorthy, K.; Pazhamalai, P.; Mariappan, V.K.; Manoharan, S.; Kim, S.-J. High performance self-charging supercapacitors using a porous PVDF-ionic liquid electrolyte sandwiched between two-dimensional graphene electrodes. *J. Mater. Chem. A* **2019**, *7*, 21693–21703. [[CrossRef](#)]
38. Sahoo, S.; Ratha, S.; Rout, C.S.; Nayak, S.K. Self-charging supercapacitors for smart electronic devices: A concise review on the recent trends and future sustainability. *J. Mater. Sci.* **2022**, *57*, 4399–4440. [[CrossRef](#)]
39. Wu, Z.; Cheng, T.; Wang, Z.L. Self-Powered Sensors and Systems Based on Nanogenerators. *Sensors* **2020**, *20*, 2925. [[CrossRef](#)]
40. Askari, H.; Hashemi, E.; Khajepour, A.; Khamesee, M.B.; Wang, Z.L. Towards self-powered sensing using nanogenerators for automotive systems. *Nano Energy* **2018**, *53*, 1003–1019. [[CrossRef](#)]
41. Aaryashree; Sahoo, S.; Walke, P.; Nayak, S.K.; Rout, C.S.; Late, D.J. Recent developments in self-powered smart chemical sensors for wearable electronics. *Nano Res.* **2021**, *14*, 3669–3689. [[CrossRef](#)]
42. Hu, Y.; Zhang, M.; Qin, C.; Qian, X.; Zhang, L.; Zhou, J.; Lu, A. Transparent, conductive cellulose hydrogel for flexible sensor and triboelectric nanogenerator at subzero temperature. *Carbohydr. Polym.* **2021**, *265*, 118078. [[CrossRef](#)] [[PubMed](#)]
43. Wu, Y.; Qu, J.; Zhang, X.; Ao, K.; Zhou, Z.; Zheng, Z.; Mu, Y.; Wu, X.; Luo, Y.; Feng, S.-P. Biomechanical Energy Harvesters Based on Ionic Conductive Organohydrogels via the Hofmeister Effect and Electrostatic Interaction. *ACS Nano* **2021**, *15*, 13427–13435. [[CrossRef](#)] [[PubMed](#)]
44. Zhao, K.; Lv, H.; Meng, J.; Song, Z.; Meng, C.; Liu, M.; Zhang, D. Triboelectrification-Induced Electricity in Self-Healing Hydrogel for Mechanical Energy Harvesting and Ultra-sensitive Pressure Monitoring. *ACS Omega* **2022**, *7*, 18816–18825. [[CrossRef](#)]
45. Shin, J.; Ji, S.; Yoon, J.; Park, J. Module-Type Triboelectric Nanogenerators Capable of Harvesting Power from a Variety of Mechanical Energy Sources. *Micromachines* **2021**, *12*, 1043. [[CrossRef](#)]
46. Zhang, Y.; Cao, X.; Wang, Z.L. The sealed bionic fishtail-structured TENG based on anticorrosive paint for ocean sensor systems. *Nano Energy* **2023**, *108*, 108210. [[CrossRef](#)]
47. Wang, F.; Zhao, L.; Song, F.; Wu, J.; Zhou, Q.; Xie, L. Hybrid natural hydrogels integrated with voriconazole-loaded microspheres for ocular antifungal applications. *J. Mater. Chem. B* **2021**, *9*, 3377–3388. [[CrossRef](#)]
48. Luo, X.; Zhu, L.; Wang, Y.-C.; Li, J.; Nie, J.; Wang, Z.L. A Flexible Multifunctional Triboelectric Nanogenerator Based on MXene/PVA Hydrogel. *Adv. Funct. Mater.* **2021**, *31*, 2104928. [[CrossRef](#)]
49. Li, R.; Xu, Z.; Li, L.; Wei, J.; Wang, W.; Yan, Z.; Chen, T. Breakage-resistant hydrogel electrode enables ultrahigh mechanical reliability for triboelectric nanogenerators. *Chem. Eng. J.* **2023**, *454*, 140261. [[CrossRef](#)]
50. Wang, L.; Daoud, W.A. Hybrid conductive hydrogels for washable human motion energy harvester and self-powered temperature-stress dual sensor. *Nano Energy* **2019**, *66*, 104080. [[CrossRef](#)]
51. Jing, X.; Li, H.; Mi, H.-Y.; Feng, P.-Y.; Tao, X.; Liu, Y.; Liu, C.; Shen, C. A flexible semitransparent dual-electrode hydrogel based triboelectric nanogenerator with tough interfacial bonding and high energy output. *J. Mater. Chem. C* **2020**, *8*, 5752–5760. [[CrossRef](#)]
52. Xiao, Z.; Luo, Y.; Yuan, H.; Zheng, T.; Xu, S.; Dai, G.; Yang, J. Coupling charge pump and BUCK circuits to efficiently enhance the output performance of triboelectric nanogenerator. *Nano Energy* **2023**, *115*, 108749. [[CrossRef](#)]
53. Shi, M.; Yang, W.; Zhang, Z.; Zhao, M.; Wang, Z.L.; Lu, X. Hydrogels with highly concentrated salt solution as electrolytes for solid-state supercapacitors with a suppressed self-discharge rate. *J. Mater. Chem. A* **2022**, *10*, 2966–2972. [[CrossRef](#)]
54. Abir, S.S.H.; Sadaf, M.U.K.; Saha, S.K.; Touhami, A.; Lozano, K.; Uddin, M.J. Nanofiber-Based Substrate for a Triboelectric Nanogenerator: High-Performance Flexible Energy Fiber Mats. *ACS Appl. Mater. Interfaces* **2021**, *13*, 60401–60412. [[CrossRef](#)]
55. Bagchi, B.; Datta, P.; Fernandez, C.S.; Gupta, P.; Jaufuraully, S.; David, A.L.; Siassakos, D.; Desjardins, A.; Tiwari, M.K. Flexible triboelectric nanogenerators using transparent copper nanowire electrodes: Energy harvesting, sensing human activities and material recognition. *Mater. Horiz.* **2023**, *10*, 3124–3134. [[CrossRef](#)]
56. Fan, J.; Yuan, M.; Wang, L.; Xia, Q.; Zheng, H.; Zhou, A. MXene supported by cotton fabric as electrode layer of triboelectric nanogenerators for flexible sensors. *Nano Energy* **2023**, *105*, 107973. [[CrossRef](#)]
57. Wang, G.; Liu, X.; Wang, Y.; Zheng, Z.; Zhu, Z.; Yin, Y.; Zhu, L.; Wang, X. Energy Harvesting and Sensing Integrated Woven Structure Kneepad Based on Triboelectric Nanogenerators. *Adv. Mater. Technol.* **2023**, *8*, 2200973. [[CrossRef](#)]
58. Xiong, Y.; Luo, L.; Yang, J.; Han, J.; Liu, Y.; Jiao, H.; Wu, S.; Cheng, L.; Feng, Z.; Sun, J.; et al. Scalable spinning, winding, and knitting graphene textile TENG for energy harvesting and human motion recognition. *Nano Energy* **2023**, *107*, 108137. [[CrossRef](#)]
59. Li, Z.; Li, C.; Sun, W.; Bai, Y.; Li, Z.; Deng, Y. A Controlled Biodegradable Triboelectric Nanogenerator Based on PEGDA/Laponite Hydrogels. *ACS Appl. Mater. Interfaces* **2023**, *15*, 12787–12796. [[CrossRef](#)]
60. Zhang, H.; Zhang, D.; Wang, Z.; Xi, G.; Mao, R.; Ma, Y.; Wang, D.; Tang, M.; Xu, Z.; Luan, H. Ultrastretchable, Self-Healing Conductive Hydrogel-Based Triboelectric Nanogenerators for Human-Computer Interaction. *ACS Appl. Mater. Interfaces* **2023**, *15*, 5128–5138. [[CrossRef](#)]
61. Qu, M.; Shen, L.; Wang, J.; Zhang, N.; Pang, Y.; Wu, Y.; Ge, J.; Peng, L.; Yang, J.; He, J. Superhydrophobic, Humidity-Resistant, and Flexible Triboelectric Nanogenerators for Biomechanical Energy Harvesting and Wearable Self-Powered Sensing. *ACS Appl. Nano Mater.* **2022**, *5*, 9840–9851. [[CrossRef](#)]
62. Rahman, M.T.; Rahman, M.S.; Kumar, H.; Kim, K.; Kim, S. Metal-Organic Framework Reinforced Highly Stretchable and Durable Conductive Hydrogel-Based Triboelectric Nanogenerator for Biomotion Sensing and Wearable Human-Machine Interfaces. *Adv. Funct. Mater.* **2023**, 2303471. [[CrossRef](#)]

63. Ma, B.; Cheng, L.; Bai, S.; Jia, X.; Ma, J.; Zhao, J.; Wang, L.; Qin, Y. 3D spirally coiled piezoelectric nanogenerator for large impact energy harvesting. *Nano Energy* **2023**, *111*, 108412. [[CrossRef](#)]
64. Zhou, X.; Parida, K.; Chen, J.; Xiong, J.; Zhou, Z.; Jiang, F.; Xin, Y.; Magdassi, S.; Lee, P.S. 3D Printed Auxetic Structure-Assisted Piezoelectric Energy Harvesting and Sensing. *Adv. Energy Mater.* **2023**, *13*, 2301159. [[CrossRef](#)]
65. Zong, Y.; Wang, R.; Xu, S.; Zhang, R.; Zhang, Z. Flexible Piezoelectric Nanogenerator Based on Cellulose Nanofibril/MXene Composite Aerogels for Low-Frequency Energy Harvesting. *ACS Appl. Nano Mater.* **2023**, *6*, 9021–9031. [[CrossRef](#)]
66. Wang, Y.; Zhu, L.; Du, C. Progress in Piezoelectric Nanogenerators Based on PVDF Composite Films. *Micromachines* **2021**, *12*, 1278. [[CrossRef](#)]
67. Yi, J.; Song, Y.; Cao, Z.; Li, C.; Xiong, C. Gram-scale Y-doped ZnO and PVDF electrospun film for piezoelectric nanogenerators. *Compos. Sci. Technol.* **2021**, *215*, 109011. [[CrossRef](#)]
68. Chen, H.; Zhou, L.; Fang, Z.; Wang, S.; Yang, T.; Zhu, L.; Hou, X.; Wang, H.; Wang, Z.L. Piezoelectric Nanogenerator Based on In Situ Growth All-Inorganic CsPbBr<sub>3</sub> Perovskite Nanocrystals in PVDF Fibers with Long-Term Stability. *Adv. Funct. Mater.* **2021**, *31*, 2011073. [[CrossRef](#)]
69. Yang, J.; Zhang, Y.; Li, Y.; Wang, Z.; Wang, W.; An, Q.; Tong, W. Piezoelectric Nanogenerators based on Graphene Oxide/PVDF Electrospun Nanofiber with Enhanced Performances by In-Situ Reduction. *Mater. Today Commun.* **2021**, *26*, 101629. [[CrossRef](#)]
70. Wang, L.; Yu, Y.; Zhao, X.; Zhang, Z.; Yuan, X.; Cao, J.; Meng, W.; Ye, L.; Lin, W.; Wang, G. A Biocompatible Self-Powered Piezoelectric Poly(vinyl alcohol)-Based Hydrogel for Diabetic Wound Repair. *ACS Appl. Mater. Interfaces* **2022**, *14*, 46273–46289. [[CrossRef](#)]
71. Chen, Y.; Xu, W.; Zheng, X.; Huang, X.; Dan, N.; Wang, M.; Li, Y.; Li, Z.; Dan, W.; Wang, Y. Two-Layered Biomimetic Flexible Self-Powered Electrical Stimulator for Promoting Wound Healing. *Biomacromolecules* **2023**, *24*, 1483–1496. [[CrossRef](#)] [[PubMed](#)]
72. Ge, Z.; Qiao, Y.; Zhu, W.; Xu, Y.; Fang, Q.; Wang, D.; Tang, Y.; Zhao, R.; Deng, X.; Lin, W.; et al. Highly stretchable polyester-based piezoelectric elastomer for simultaneously realization of accelerated regeneration and motion monitoring for Achilles tendon rupture. *Nano Energy* **2023**, *115*, 108751. [[CrossRef](#)]
73. Pi, W.; Rao, F.; Cao, J.; Zhang, M.; Chang, T.; Han, Y.; Zheng, Y.; Liu, S.; Li, Q.; Sun, X.; et al. Sono-electro-mechanical therapy for peripheral nerve regeneration through piezoelectric nanotracts. *Nano Today* **2023**, *50*, 101860. [[CrossRef](#)]
74. Xie, T.; Liu, Q.; Xue, G.; Zhang, Y.; Zhou, J.; Zhu, Z.; Gou, X. Experimental-numerical analysis of cell adhesion-mediated electromechanical stimulation on piezoelectric nanofiber scaffolds. *J. Biomech.* **2021**, *129*, 110777. [[CrossRef](#)]
75. Yang, S.; Wang, Y.; Liang, X. Piezoelectric Nanomaterials Activated by Ultrasound in Disease Treatment. *Pharmaceutics* **2023**, *15*, 1338. [[CrossRef](#)]
76. Zhan, L.; Xiao, C.; Li, C.; Zhai, J.; Yang, F.; Piao, J.; Ning, C.; Zhou, Z.; Yu, P.; Qi, S. Internal Wireless Electrical Stimulation from Piezoelectric Barium Titanate Nanoparticles as a New Strategy for the Treatment of Triple-Negative Breast Cancer. *ACS Appl. Mater. Interfaces* **2022**, *14*, 45032–45041. [[CrossRef](#)]
77. Dupont, M.F.; MacFarlane, D.R.; Pringle, J.M. Thermo-electrochemical cells for waste heat harvesting-progress and perspectives. *Chem. Commun.* **2017**, *53*, 6288–6302. [[CrossRef](#)]
78. Siddique, A.R.M.; Mahmud, S.; Heyst, B.V. A review of the state of the science on wearable thermoelectric power generators (TEGs) and their existing challenges. *Renew. Sustain. Energy Rev.* **2017**, *73*, 730–744. [[CrossRef](#)]
79. Anand, S.; Gurunathan, R.; Soldi, T.; Borgsmiller, L.; Orenstein, R.; Snyder, G.J. Thermoelectric transport of semiconductor full-Heusler VFe<sub>2</sub>Al. *J. Mater. Chem. C* **2020**, *8*, 10174–10184. [[CrossRef](#)]
80. Fan, T.; Xie, C.; Wang, S.; Oganov, A.R.; Cheng, L. First-principles study of thermoelectric properties of Mg<sub>2</sub>Si-Mg<sub>2</sub>Pb semiconductor materials. *RSC Adv.* **2018**, *8*, 17168–17175. [[CrossRef](#)]
81. Zhang, H.; Zhang, Y.; Yu, P.; Wang, L.-M.; Li, G. Preparation and thermoelectric properties of novel Tellurium-based glassy semiconductors. *Scr. Mater.* **2021**, *203*, 114038. [[CrossRef](#)]
82. Zhang, J.; Dong, Z.; Tan, S.; Li, Y.; Zhang, J.; Zhang, W.; Luo, J. Designing vacancy-filled Heusler thermoelectric semiconductors by the Slater-Pauling rule. *Mater. Today Energy* **2022**, *27*, 101035. [[CrossRef](#)]
83. Zheng, S.; Xiao, S.; Peng, K.; Pan, Y.; Yang, X.; Lu, X.; Han, G.; Zhang, B.; Zhou, Z.; Wang, G.; et al. Symmetry-Guaranteed High Carrier Mobility in Quasi-2D Thermoelectric Semiconductors. *Adv. Mater.* **2023**, *35*, 2210380. [[CrossRef](#)] [[PubMed](#)]
84. Saberi, Y.; Sajjadi, S.A.; Mansouri, H. Comparison of thermoelectric properties of Bi<sub>2</sub>Te<sub>3</sub> and Bi<sub>2</sub>Se<sub>0.3</sub>Te<sub>2.7</sub> thin film materials synthesized by hydrothermal process and thermal evaporation. *Ceram. Int.* **2021**, *47*, 11547–11559. [[CrossRef](#)]
85. Yuan, X.; Li, Z.; Shao, Y.; Yang, D.; Hu, K.; You, H.; Xu, Z.; Hua, S.; Liu, W.; Peng, P.; et al. Bi<sub>2</sub>Te<sub>3</sub>-based wearable thermoelectric generator with high power density: From structure design to application. *J. Mater. Chem. C* **2022**, *10*, 6456–6463. [[CrossRef](#)]
86. Li, J.; Xu, T.; Ma, Z.; Li, W.; Qian, Y.; Tao, Y.; Wei, Y.; Jiang, Q.; Luo, Y.; Yang, J. Self-Healable and Stretchable PAAc/XG/Bi<sub>2</sub>Se<sub>0.3</sub>Te<sub>2.7</sub> Hybrid Hydrogel Thermoelectric Materials. *Energy Environ. Mater.* **2022**, e12547. [[CrossRef](#)]
87. Chai, X.; Tang, J.; Li, Y.; Cao, Y.; Chen, X.; Chen, T.; Zhang, Z. Highly Stretchable and Stimulus-Free Self-Healing Hydrogels with Multiple Signal Detection Performance for Self-Powered Wearable Temperature Sensors. *ACS Appl. Mater. Interfaces* **2023**, *15*, 18262–18271. [[CrossRef](#)]
88. He, Y.; Zhang, Q.; Cheng, H.; Liu, Y.; Shu, Y.; Geng, Y.; Zheng, Y.; Qin, B.; Zhou, Y.; Chen, S.; et al. Role of Ions in Hydrogels with an Ionic Seebeck Coefficient of 52.9 mV K<sup>-1</sup>. *J. Phys. Chem. Lett.* **2022**, *13*, 4621–4627. [[CrossRef](#)]
89. Tian, C.; Bai, C.; Wang, T.; Yan, Z.; Zhang, Z.; Zhuo, K.; Zhang, H. Thermogalvanic hydrogel electrolyte for harvesting biothermal energy enabled by a novel redox couple of SO<sub>4</sub>/3<sup>2-</sup> ions. *Nano Energy* **2023**, *106*, 108077. [[CrossRef](#)]

90. Han, C.-G.; Qian, X.; Li, Q.; Deng, B.; Zhu, Y.; Han, Z.; Zhang, W.; Wang, W.; Feng, S.-P.; Chen, G.; et al. Giant thermopower of ionic gelatin near room temperature. *Science* **2020**, *368*, 1091–1098. [[CrossRef](#)]
91. Lei, Z.; Gao, W.; Wu, P. Double-network thermocells with extraordinary toughness and boosted power density for continuous heat harvesting. *Joule* **2021**, *5*, 2211–2222. [[CrossRef](#)]
92. Li, N.; Khan, S.A.; Yang, K.; Zhuo, K.; Zhang, Y.; Zhang, H. A self-powered thermogalvanic organohydrogel-based touch-to-speech Braille transmission interface with temperature resistance and stretchability. *Compos. Sci. Technol.* **2023**, *239*, 110077. [[CrossRef](#)]
93. Bai, C.; Wang, Z.; Yang, S.; Cui, X.; Li, X.; Yin, Y.; Zhang, M.; Wang, T.; Sang, S.; Zhang, W.; et al. Wearable Electronics Based on the Gel Thermogalvanic Electrolyte for Self-Powered Human Health Monitoring. *ACS Appl. Mater. Interfaces* **2021**, *13*, 37316–37322. [[CrossRef](#)]
94. Zhang, L.; Fang, R.; Li, X.; Tian, C.; Li, J.; Cui, X.; Zhang, H. Self-powered physiological monitoring strategy enabled by adaptive dual-network thermogalvanic hydrogels. *Sens. Actuators A* **2023**, *361*, 114604. [[CrossRef](#)]
95. Xu, C.; Sun, Y.; Zhang, J.; Xu, W.; Tian, H. Adaptable and Wearable Thermocell Based on Stretchable Hydrogel for Body Heat Harvesting. *Adv. Energy Mater.* **2022**, *12*, 2201542. [[CrossRef](#)]
96. Han, Y.; Wei, H.; Du, Y.; Li, Z.; Feng, S.-P.; Huang, B.; Xu, D. Ultrasensitive Flexible Thermal Sensor Arrays based on High-Thermopower Ionic Thermoelectric Hydrogel. *Adv. Sci.* **2023**, *10*, 2302685. [[CrossRef](#)] [[PubMed](#)]
97. Chen, X.; Han, M.; Chen, H.; Cheng, X.; Song, Y.; Su, Z.; Jiang, Y.; Zhang, H. A wave-shaped hybrid piezoelectric and triboelectric nanogenerator based on P(VDF-TrFE) nanofibers. *Nanoscale* **2017**, *9*, 1263–1270. [[CrossRef](#)]
98. Li, X.; Ji, D.; Yu, B.; Ghosh, R.; He, J.; Qin, X.; Ramakrishna, S. Boosting piezoelectric and triboelectric effects of PVDF nanofiber through carbon-coated piezoelectric nanoparticles for highly sensitive wearable sensors. *Chem. Eng. J.* **2021**, *426*, 130345. [[CrossRef](#)]
99. Wang, S.; Tong, W.; Li, Y.; Zhang, P.; Liu, Y.; Chen, Y.; Zhang, Y. Contributions of piezoelectricity and triboelectricity to a hydroxyapatite/PVDF-HFP fiber-film nanogenerator. *Nano Energy* **2023**, *105*, 108026. [[CrossRef](#)]
100. Yang, X.; Daoud, W.A. Triboelectric and Piezoelectric Effects in a Combined Tribo-Piezoelectric Nanogenerator Based on an Interfacial ZnO Nanostructure. *Adv. Funct. Mater.* **2016**, *26*, 8194–8201. [[CrossRef](#)]
101. Li, J.; Liu, J.; Peng, C.; Liu, X.; Wu, Z.; Zheng, F. Design and Testing of a Non-Contact MEMS Voltage Sensor Based on Single-Crystal Silicon Piezoresistive Effect. *Micromachines* **2022**, *13*, 619. [[CrossRef](#)] [[PubMed](#)]
102. Li, Y.; Liang, T.; Lei, C.; Li, Q.; Li, Z.; Ghaffar, A.; Xiong, J. Study on the Stability of the Electrical Connection of High-Temperature Pressure Sensor Based on the Piezoresistive Effect of P-Type SiC. *Micromachines* **2021**, *12*, 216. [[CrossRef](#)] [[PubMed](#)]
103. Tian, B.; Shang, H.; Wang, D.; Liu, Y.; Wang, W. Investigation on Piezoresistive Effect of n-Type 4H-SiC Based on All-SiC Pressure Sensors. *IEEE Sens. J.* **2022**, *22*, 6435–6441. [[CrossRef](#)]
104. Wu, C.; Fang, X.; Kang, Q.; Fang, Z.; Wu, J.; He, H.; Zhang, D.; Zhao, L.; Tian, B.; Maeda, R.; et al. Exploring the nonlinear piezoresistive effect of 4H-SiC and developing MEMS pressure sensors for extreme environments. *Microsyst. Nanoeng.* **2023**, *9*, 41. [[CrossRef](#)]
105. Lyu, C.; Wen, B.; Bai, Y.; Luo, D.; Wang, X.; Zhang, Q.; Xing, C.; Kong, T.; Diao, D.; Zhang, X. Bone-inspired (GNEC/HAPAAm) hydrogel with fatigue-resistance for use in underwater robots and highly piezoresistive sensors. *Microsyst. Nanoeng.* **2023**, *9*, 99. [[CrossRef](#)] [[PubMed](#)]
106. Shen, X.; Zheng, L.; Tang, R.; Nie, K.; Wang, Z.; Jin, C.; Sun, Q. Double-Network Hierarchical-Porous Piezoresistive Nanocomposite Hydrogel Sensors Based on Compressive Cellulosic Hydrogels Deposited with Silver Nanoparticles. *ACS Sustain. Chem. Eng.* **2020**, *8*, 7480–7488. [[CrossRef](#)]
107. Xia Zhang, Y.; He, Y.; Liang, Y.; Tang, J.; Yang, Y.; Ming Song, H.; Zrinyi, M.; Mei Chen, Y. Sensitive piezoresistive pressure sensor based on micropyrnid patterned tough hydrogel. *Appl. Surf. Sci.* **2023**, *615*, 156328. [[CrossRef](#)]
108. Zhang, H.; Yan, Q.; Horvat, J.; Lewis, R.A. Piezoresistive and Electrical Properties of a Catecholic Amino Acid-Polyacrylamide Single-Walled Carbon Nanotube Hydrogel Hybrid Network. *ACS Appl. Polym. Mater.* **2021**, *3*, 671–678. [[CrossRef](#)]
109. Wang, Z.; Liu, Z.; Zhao, G.; Zhang, Z.; Zhao, X.; Wan, X.; Zhang, Y.; Wang, Z.L.; Li, L. Stretchable Unsymmetrical Piezoelectric BaTiO<sub>3</sub> Composite Hydrogel for Triboelectric Nanogenerators and Multimodal Sensors. *ACS Nano* **2022**, *16*, 1661–1670. [[CrossRef](#)]
110. Cheng, P.; Wang, D.; Schaaf, P. A Review on Photothermal Conversion of Solar Energy with Nanomaterials and Nanostructures: From Fundamentals to Applications. *Adv. Sustain. Syst.* **2022**, *6*, 2200115. [[CrossRef](#)]
111. Mateo, D.; Cerrillo, J.L.; Durini, S.; Gascon, J. Fundamentals and applications of photo-thermal catalysis. *Chem. Soc. Rev.* **2021**, *50*, 2173–2210. [[CrossRef](#)] [[PubMed](#)]
112. Du, S.; Lu, Z.; Gao, L.; Ge, Y.; Xu, X.; Zhang, H. Salmonella typhimurium detector based on the intrinsic peroxidase-like activity and photothermal effect of MoS<sub>2</sub>. *Microchim. Acta* **2020**, *187*, 627. [[CrossRef](#)] [[PubMed](#)]
113. Fang, J.; Zhang, P.; Zhou, G. Hydrothermal synthesis of highly stable copper sulfide nanorods for efficient photo-thermal conversion. *Mater. Lett.* **2018**, *217*, 71–74. [[CrossRef](#)]
114. Zhao, Y.; Sadat, M.E.; Dunn, A.; Xu, H.; Chen, C.-H.; Nakasuga, W.; Ewing, R.C.; Shi, D. Photothermal effect on Fe<sub>3</sub>O<sub>4</sub> nanoparticles irradiated by white-light for energy-efficient window applications. *Sol. Energy Mater. Sol. Cells* **2017**, *161*, 247–254. [[CrossRef](#)]
115. Joseph Fortenbaugh, R.; Lear, B.J. On-demand curing of polydimethylsiloxane (PDMS) using the photothermal effect of gold nanoparticles. *Nanoscale* **2017**, *9*, 8555–8559. [[CrossRef](#)] [[PubMed](#)]

116. Yang, H.; Ahmed Khan, S.; Li, N.; Fang, R.; Huang, Z.; Zhang, H. Thermogalvanic gel patch for self-powered human motion recognition enabled by photo-thermal-electric conversion. *Chem. Eng. J.* **2023**, *473*, 145247. [[CrossRef](#)]
117. Bai, C.; Li, X.; Cui, X.; Yang, X.; Zhang, X.; Yang, K.; Wang, T.; Zhang, H. Transparent stretchable thermogalvanic PVA/gelation hydrogel electrolyte for harnessing solar energy enabled by a binary solvent strategy. *Nano Energy* **2022**, *100*, 107449. [[CrossRef](#)]
118. Gao, M.; Peh, C.K.; Phan, H.T.; Zhu, L.; Ho, G.W. Solar Absorber Gel: Localized Macro-Nano Heat Channeling for Efficient Plasmonic Au Nanoflowers Photothermic Vaporization and Triboelectric Generation. *Adv. Energy Mater.* **2018**, *8*, 1800711. [[CrossRef](#)]
119. Bai, C.; Zhang, J.; Yang, K.; Zhang, Z.; Zhang, H. A vertical stretchable self-powered light sensor based on thermogalvanic gel electrolyte via photo-thermal-electric conversion. *Sens. Actuators A* **2023**, *354*, 114305. [[CrossRef](#)]
120. Gao, F.-L.; Min, P.; Gao, X.-Z.; Li, C.; Zhang, T.; Yu, Z.-Z.; Li, X. Integrated temperature and pressure dual-mode sensors based on elastic PDMS foams decorated with thermoelectric PEDOT:PSS and carbon nanotubes for human energy harvesting and electronic-skin. *J. Mater. Chem. A* **2022**, *10*, 18256–18266. [[CrossRef](#)]
121. Horta Romarís, L.; González Rodríguez, M.V.; Huang, B.; Costa, P.; Lasagabáster Latorre, A.; Lanceros-Mendez, S.; Abad López, M.J. Multifunctional electromechanical and thermoelectric polyaniline-poly(vinyl acetate) latex composites for wearable devices. *J. Mater. Chem. C* **2018**, *6*, 8502–8512. [[CrossRef](#)]
122. Gao, X.-Z.; Gao, F.-L.; Liu, J.; Li, Y.; Wan, P.; Yu, Z.-Z.; Li, X. Self-Powered Resilient Porous Sensors with Thermoelectric Poly(3,4-ethylenedioxythiophene):Poly(styrenesulfonate) and Carbon Nanotubes for Sensitive Temperature and Pressure Dual-Mode Sensing. *ACS Appl. Mater. Interfaces* **2022**, *14*, 43783–43791. [[CrossRef](#)] [[PubMed](#)]
123. Fu, X.; Zhuang, Z.; Zhao, Y.; Liu, B.; Liao, Y.; Yu, Z.; Yang, P.; Liu, K. Stretchable and Self-Powered Temperature-Pressure Dual Sensing Ionic Skins Based on Thermogalvanic Hydrogels. *ACS Appl. Mater. Interfaces* **2022**, *14*, 44792–44798. [[CrossRef](#)] [[PubMed](#)]

**Disclaimer/Publisher's Note:** The statements, opinions and data contained in all publications are solely those of the individual author(s) and contributor(s) and not of MDPI and/or the editor(s). MDPI and/or the editor(s) disclaim responsibility for any injury to people or property resulting from any ideas, methods, instructions or products referred to in the content.